The Clinically Used Iron Chelator Deferasirox is an Inhibitor of Epigenetic JumonjiC Domain-Containing Histone Demethylases

Martin Roatsch,[a,†] Inga Hoffmann,[a] Martine I. Abboud,[b] Rebecca L. Hancock,[b] Hanna Tarhonskaya,[b] Kuo-Feng Hsu,[b] Sarah E. Wilkins,[b] Tzu-Lan Yeh,[b] Kerstin Lippl,[b] Kerstin Serrer,[c] Isabelle Moneke,[d] Theresa D. Ahrens,[e] Dina Robaa,[f] Sandra Wenzler,[a] Nicolas P. F. Barthes,[a] Henriette Franz,[g] Wolfgang Sippl,[f] Silke Lassmann,[e] Sven Diederichs,[d,h] Erik Schleicher,[c] Christopher J. Schofield,[b] Akane Kawamura,[b] Roland Schüle,[g] Manfred Jung[a]*

a. Institute of Pharmaceutical Sciences, Albert-Ludwigs-Universität Freiburg, Albertstraße 25, 79104 Freiburg i.Br., Germany

b. Chemistry Research Laboratory, University of Oxford, 12 Mansfield Road, Oxford, OX1 3TA, United Kingdom

c. Institute of Physical Chemistry, Albert-Ludwigs-Universität Freiburg, Albertstraße 21, 79104 Freiburg i.Br., Germany

d. Division of Cancer Research, Department of Thoracic Surgery, Medical Center – University of Freiburg, Faculty of Medicine, University of Freiburg, German Cancer Consortium (DKTK) – Partner Site Freiburg, Breisacher Straße 115, 79106 Freiburg i.Br., Germany

e. Institute for Surgical Pathology, Medical Center and Faculty of Medicine – University of Freiburg, Breisacher Straße 115a, 79106 Freiburg i.Br., Germany

f. Institute of Pharmacy, Martin-Luther-University Halle-Wittenberg, Wolfgang-Langenbeck-Straße 4, 06120 Halle (Saale), Germany

g. Central Clinical Research, Medical Center and Faculty of Medicine – University of Freiburg, Breisacher Straße 66, 79106 Freiburg i.Br., Germany

h. Division of RNA Biology & Cancer, German Cancer Research Center (DKFZ), Im Neuenheimer Feld 280, 69120 Heidelberg, Germany

ABSTRACT. Fe(II)- and 2-oxoglutarate (2OG)-dependent JumonjiC domain-containing histone demethylases (JmjC KDMs) are 'epigenetic eraser' enzymes involved in the regulation of gene expression and are emerging drug targets in oncology. We screened a set of clinically used iron chelators and report that they potently inhibit JMJD2A (KDM4A) *in vitro*. Mode of action investigations revealed that one compound, deferasirox, is a *bona fide* active site-binding inhibitor as shown by kinetic and spectroscopic studies. Synthesis of derivatives with improved cell permeability resulted in significant upregulation of histone trimethylation and potent cancer cell growth inhibition. Deferasirox was also found to inhibit human 2OG-dependent hypoxia inducible factor prolyl hydroxylase activity. Therapeutic effects of clinically used deferasirox may thus involve transcriptional regulation through 2OG oxygenase inhibition. Deferasirox might provide a useful starting point for the development of novel anticancer drugs targeting 2OG oxygenases and a valuable tool compound for investigations of KDM function.

KEYWORDS

epigenetics • histone demethylase • inhibitor • off-target • clinically used drugs • deferasirox • Jumonji • hypoxia • 2-oxoglutarate oxygenase

INTRODUCTION. Posttranslational modifications of histone proteins, such as lysine methylation, are a vital mechanism of epigenetic gene regulation in cells.[1, 2] These 'marks' are deposited by histone methyltransferases (HMTs) and removed by lysine demethylases (KDMs), of which two mechanistically different classes are known.[1] While LSD1 (KDM1A) demethylates histones in an FAD-dependent reaction, the much larger class of JumonjiC domain-containing histone demethylases (JmjC KDMs), discovered in 2006, are Fe(II)- and 2-oxoglutarate (2OG)-dependent oxygenases. Demethylation proceeds with an oxidative mechanism *via* formation of an unstable hemiaminal intermediate, which decomposes to formaldehyde and the demethylated lysine residue (Figure 1a).[3-5]

Overexpression of JmjC demethylase genes is linked to diseases,[6] in particular cancer, with the $H3K9me_3$ and $H3K36me_3$ demethylase JMJD2A (KDM4A), a member of the KDM4 subfamily (subtypes A-E), being a prominent example. Elevated levels of JMJD2A have been detected in human malignancies including breast,[7, 8] prostate,[9] bladder,[10] colorectal,[11] and lung[12] cancers. In breast and prostate hormone-dependent cancers, JMJD2A is implicated as a co-activator of the estrogen and androgen receptors, respectively.[7-9] Conversely, in malignant urothelium, lowered JMJD2A levels correlate with poor prognosis.[13] The contrasting roles of JMJD2A in human disease have recently been discussed.[14] As JumonjiC KDMs use molecular oxygen as oxidizing agent for the demethylation reaction, a role in cellular oxygen sensing has also been discussed, e. g. for the subtype KDM6A.[15]

JmjC histone demethylases have emerged as promising drug targets,[1, 16-20] with inhibitor discovery programs being reported by us[21-27] and others,[28-35] as recently reviewed.[17, 19, 36-40] The majority of reported JmjC KDM inhibitors function by active site metal chelation and competitive displacement of the co-substrate 2OG.[36-39] Very recently, covalent KDM5

inhibitors[41, 42] and inhibitors of both the lysyl- and arginyl-demethylase activities[43] have also been reported.

We were, therefore, interested in investigating the effect of clinically used iron chelating drugs on KDM activity. These compounds are used to treat patients with excess levels of iron ions in their blood (hemochromatosis). Currently, three such molecules are in clinical use, namely deferoxamine **1**, deferiprone **2**, and deferasirox **3a** (Figure 1b).[44, 45] For our tests, we used two established *in vitro* screening assays with orthogonal read-outs as previously reported,[21-23] namely the enzyme-coupled formaldehyde dehydrogenase (FDH)-coupled fluorescence intensity assay and the commercial antibody-based TR-FRET LANCE*Ultra* assay.

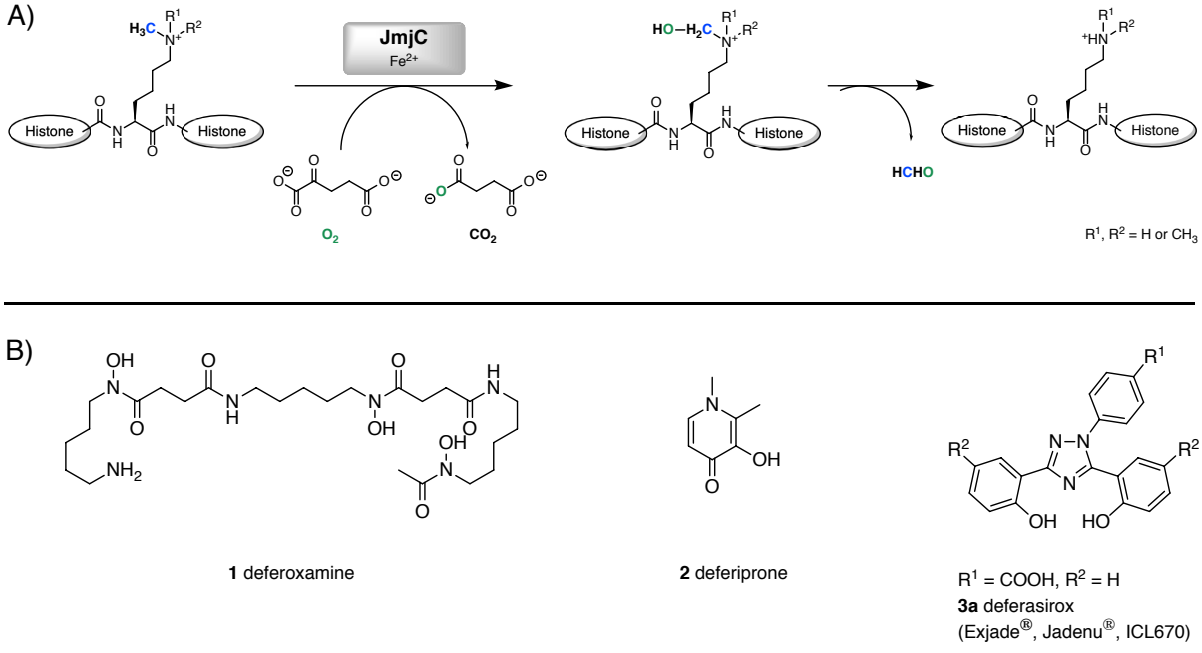

Figure 1. a) Iron(II)- and 2-oxoglutarate-dependent demethylation reaction catalyzed by JmjC KDMs. b) Chemical structures of investigated clinically used iron chelators **1**-**3a**.

RESULTS AND DISCUSSION. Intriguingly, all three compounds **1**-**3a** showed potent inhibition of demethylation of H3K9me$_3$ peptides by JMJD2A in these *in vitro* assays with IC_{50} values between 3 and 17 μM (Table 1). The potency of inhibition is in a comparable range to that of the well-known JmjC inhibitor JIB-04,[33, 46] which was used as reference compound. Inhibition of JMJD2A and the closely related subtype JMJD2B by **1** and **3** was confirmed using a mass spectrometry (MS) assay (Supporting Table 1). In a very recent publication, data was presented implicated that deferiprone **2** and derivatives thereof inhibited some KDMs with comparable potency.[47] In contrast to our findings, the authors report no inhibition of the KDM4 subfamily, but of selected members of other subfamilies. A different *in vitro* assay was used than in our set-up, which can potentially explain the observed differences as KDM inhibition is highly sensitive to co-factor Fe^{2+} and co-substrate 2OG concentrations. We aimed to study to what extent the observed inhibition by metal chelators was bona fide inhibition of the enzyme by active site binding of the molecules or non-specific inhibition arising from sequestration of iron ions in the assay buffer or extraction of metal ions from the protein, i.e. either Fe^{2+} from the active site or of the structural Zn^{2+} present in some JmjC KDM subtypes.[48] To investigate this, we varied the Fe^{2+} concentration in all assays (Supporting Table 2), but the results were inconclusive.

Table 1. *In vitro* inhibition of JMJD2A by iron chelators, the reference JmjC inhibitor JIB-04 and control compounds.[a] n. d. – not determined. n. i. – no inhibition.

Compound	R^1	R^2	FDH assay IC_{50} / μM	LANCE*Ultra* assay IC_{50} / μM
1	--	--	3.22 ± 0.30	3.33 ± 0.48
2	--	--	17.4 ± 0.8	3.87 ± 0.27
3a	COOH	H	7.37 ± 1.58	4.76 ± 0.23
3b	H	H	6.17 ± 1.43	5.27 ± 1.00
3c	COOMe	H	7.77 ± 1.32	4.12 ± 0.13
3d	COOH	Cl	14.0 ± 3.1	5.12 ± 0.05
3e	COOH	OMe	5.51 ± 0.37	3.66 ± 0.11
3f	COOH	F	5.49 ± 1.59	4.20 ± 0.22
JIB-04	--	--	17.6	4.12 ± 0.39
12a			n. d.	67% inhib. @ 100 μM
12b			n. d.	n. i. @ 100 μM

[a] Data shown are mean ± s. d. of at least two independent experiments.

To further investigate the mechanism of inhibition, we performed enzyme kinetic analyses. The results showed that only inhibition by deferasirox **3a** was, at least in part, competitive with the co-substrate 2OG (Supporting Figure 1), indicating that inhibition can stem from active site binding. With different mechanisms of inhibition likely occurring simultaneously, interpretation of the kinetic data is further complicated by background Fe^{2+} chelation as JmjC KDMs do not efficiently bind 2OG in the absence of Fe^{2+}. By contrast, inhibition by deferoxamine **1** and deferiprone **2** was not competitive with 2OG in our experiments (Supporting Figure 2), consistent with inhibition occurring only by Fe^{2+} chelation in solution. The recent report of KDM inhibition by deferiprone **2** also included docking poses of **2** in the active sites of some KDMs.[47]

Our results highlight, however, that this does not necessarily also imply a 2OG-competitive inhibition mechanism as evidenced by our kinetic data, again underlining the complexity of inhibition with regard to iron chelation.

We then adapted the LANCE*Ultra* assay system for the related subtypes JARID1A (KDM5A) and JMJD3 (KDM6B) and their respective substrates H3K4me$_3$ and H3K27me$_3$ for selectivity studies. We observed potent inhibition of these enzymes as well (Table 2), implying general inhibition of the JmjC KDMs by the entire set of clinically used iron chelators. The lack of selectivity for specific KDMs may be a challenge in the further development of these inhibitors for therapeutic use. On the other hand, many JmjC KDM inhibitors published to date, including reference inhibitor JIB-04, exhibit no or only limited selectivity for certain subfamilies, while selective inhibition of individual enzyme subtypes remains challenging.[36]

Table 2. *In vitro* inhibition of other KDM subtypes in LANCE*Ultra* assays by iron chelators and reference JMJ inhibitor JIB-04.[a]

Compound	JMJD2A (KDM4A) IC_{50} / μM	JARID1A (KDM5A) IC_{50} / μM	JMJD3 (KDM6B) IC_{50} / μM
1	3.33 ± 0.48	4.62 ± 0.27	2.36 ± 0.23
3a	4.76 ± 0.23	5.00 ± 0.62	3.95 ± 0.65
JIB-04	4.12 ± 0.39	7.20 ± 0.39	4.60 ± 0.65

[a] Data shown are mean ± s. d. of at least two independent experiments.

Further support for the hypothesis that deferasirox **3a** is a direct protein-binding inhibitor of JMJD2A comes from spectroscopic analyses. Pseudo-modulated field-sweep echo electron paramagnetic resonance (EPR) spectra of JMJD2A with Fe^{3+} bound (substituting for the

catalytically active Fe^{2+}) are shown in Figure 2 (green curve); the spectrum shows a pronounced EPR signature between 400 and 650 mT with a number of maxima and minima as is typical for nitrogen-complexed Fe^{3+}.[49-51] The presence of the EPR-visible Fe^{3+} stems from aerial oxidation of the catalytically active Fe^{2+}. Upon addition of **3a**, additional signals appeared, three of which are located between 100 and 400 mT, and one broad positive band, which is centered at around 870 mT. Clear dose dependency was observed at the marker band located at around 870 mT (orange curves in Figure 2 and Supporting Figure 3).

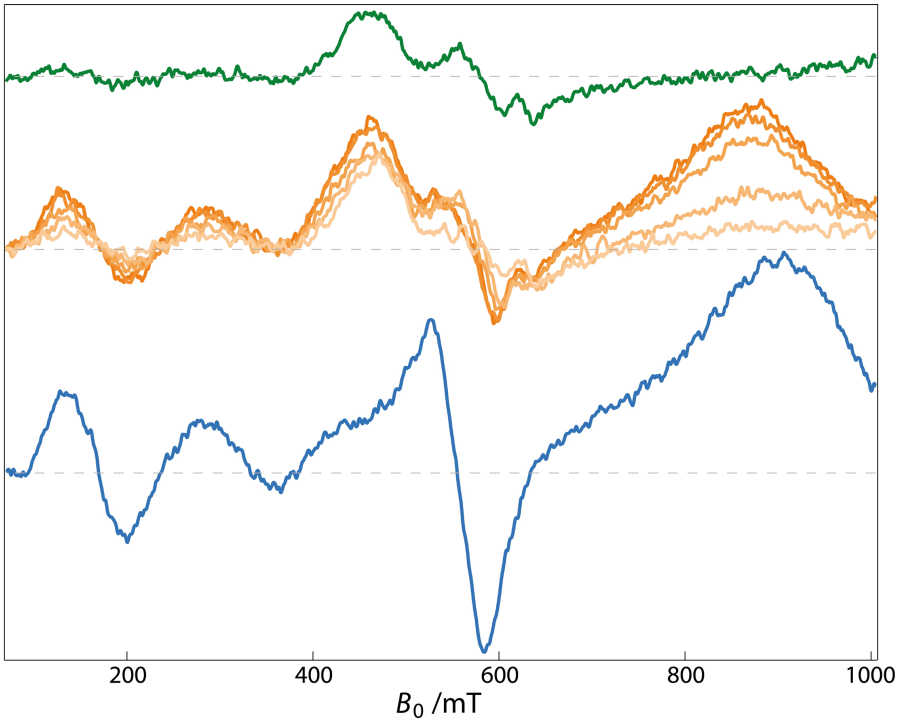

Figure 2. Pseudo-modulated field-sweep echo EPR spectra of JMJD2A in complex with Fe^{3+} without **3a** (green curve) and increasing concentrations (25, 50, 100, 150, 200 µM) of inhibitor (orange curves). The complex of **3a** and Fe^{3+} in solution results in a profoundly different spectrum (blue curve).

The EPR experiments were also performed on a sample without enzyme, but with Fe^{3+} and **3a** at a molar ratio of ~1:3. This resulted in significantly different band patterns and signal maxima (blue curve), in particular at the magnetic-field positions around 550 mT and 900 mT. The

combined results can be rationalized by invoking formation of two different Fe^{3+} complexes: one with **3a** bound to iron within the active site if enzyme is present and one with iron complexed by **3a** in solution. The formation of a complex of **3a** and Fe^{3+} within the active site of JMJD2A is supported by additional pulsed ESEEM experiments (Supporting Figure 4).

The binding of deferoxamine **1** and deferasirox **3a** to JMJD2A was further studied by NMR spectroscopy using recombinant protein. The addition of JMJD2A complexed with Zn^{2+} to a sample of **3a** led to significant line broadening and signal reduction of **3a** peaks indicating that **3a** binds to JMJD2A (Figure 3a-b). This observation is consistent with wLOGSY analyses whereby **3a** shares the same NOE sign with JMJD2A in a sample containing **3a** and JMJD2A (Figure 3c), indicating the formation of a **3a**:JMJD2A complex. By contrast, the addition of JMJD2A to a sample of **1** led to little line broadening of the deferoxamine peaks suggesting that **1** binds only relatively weakly to JMJD2A, consistent with wLOGSY experiments indicating only a weak binding event (Supporting Figure 5). Thus, under our experimental conditions, **3a** binds JMJD2A significantly more tightly than **1**.

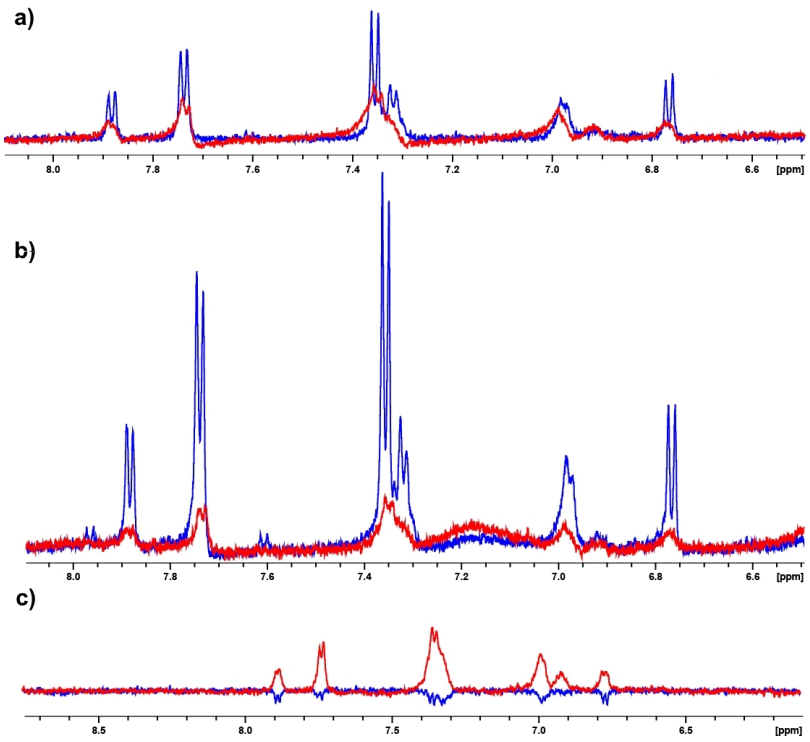

Figure 3. NMR analyses of deferasirox binding to JMJD2A (KDM4A) by a) ^{1}H excitation sculpting suppression NMR analysis, b) ^{1}H CPMG NMR analysis, and c) wLOGSY NMR analysis. Blue trace: 200 µM **3a**, red trace: 200 µM **3a** and 10 µM JMJD2A in buffer containing 50 µM Zn^{2+}.

As co-crystallization of deferasirox with JMJD2A proved unsuccessful, we further investigated the binding mode of this inhibitor by molecular docking. The suggested binding of **3a** at the active site of KDMs is corroborated by plausible binding models in JMJD2A, JARID1A, and JMJD3 (Figure 4 and Supporting Figure 6). The binding poses show that **3a** can be accommodated in the active site, chelating the Fe^{2+} ion in a tridentate manner *via* its triazole-N and both phenol-O atoms in JMJD2A and JMJD3, and in a bidentate manner *via* its triazole-N and one phenol-O in JARID1A. Additionally, viable H-bonding and hydrophobic interactions with residues of the protein binding pocket are predicted. In JMJD2A (KDM4A), **3a** is predicted to complex the central metal ion *via* one nitrogen and two phenolic oxygen atoms. One of the

phenolic rings is embedded in a hydrophobic region via π-π-stacking interactions with F185, while the phenolic-OH is able to form H-bond interactions with the histidine residue H276

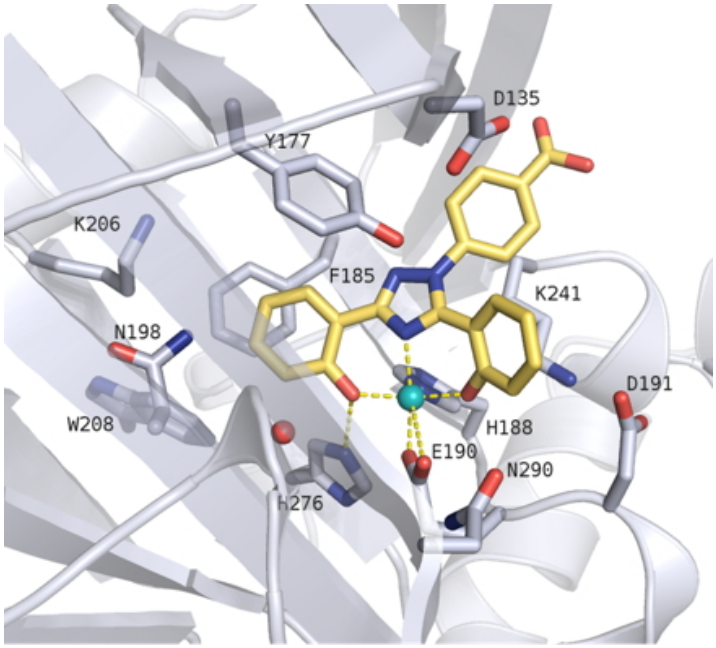

Figure 4. Molecular docking pose of **3a** in the active site of JMJD2A (KDM4A), showing that **3a** can be accommodated in the active site of this enzyme. The ligand is shown in yellow, side chains of the protein residues involved in the interaction as white sticks, water molecules and the Fe^{2+} ion as red and teal spheres, respectively. Predicted hydrogen bonds and interactions with the metal ion are depicted as yellow dashed lines.

Based on this binding model, we envisaged optimization of potency of deferasirox **3a** by the synthesis of analogs with phenol ring modifications aimed at binding to the conserved lysine residue K206 in the JMJD2A active site. The synthetic route employed (Scheme 1) followed that of reported syntheses of this structural class and the commercial deferasirox process.[52-56] This efficient two-step protocol started with condensation of appropriately substituted salicylamides **4**

and salicylic acids **5** to benzoxazinones **6** followed by condensation with the corresponding phenylhydrazines **7** to construct the central triazole ring. In the case of fluoro derivative **3f**, synthesis proceeded through the open bis(salicyl)imide form **8**, which could similarly be condensed with phenylhydrazine **7a**.

Scheme 1. Synthetic route to substituted derivatives of deferasirox **3a** and control compounds **12a**/**b**.

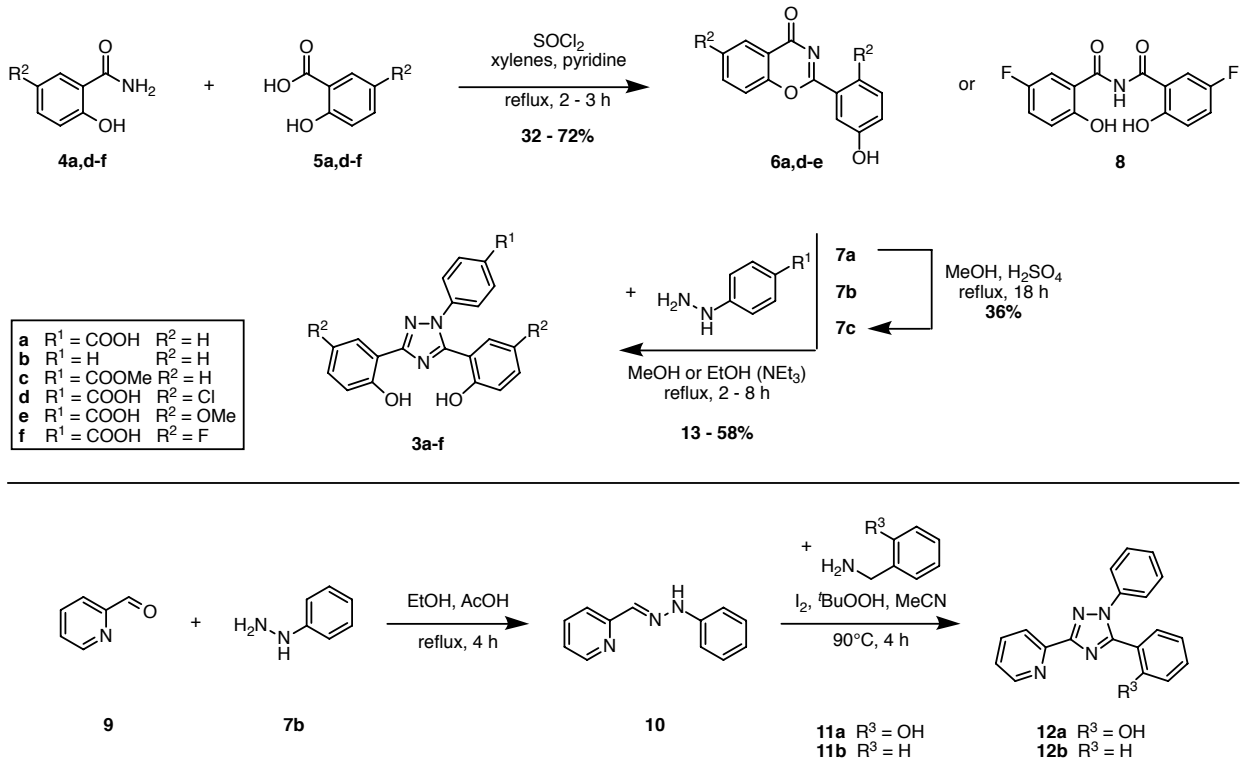

The substituted derivatives **3b-f** were tested in the *in vitro* assays against JMJD2A (Table 1) and found to be active in a concentration range similar to **3a**. In order to investigate the relevance of the tridentate iron-binding motif composed of triazole-N and two phenol-O atoms in deferasirox **3a** for potent inhibition, we designed two structural analogues **12a** and **12b**

(Scheme 1), where one or both of the phenol-O atoms have been replaced. These could synthetically be accessed by condensing picolinaldehyde **9** with phenylhydrazine **7b** and subsequent iodine-catalyzed oxidative coupling of the formed hydrazone intermediate **10** with an appropriate benzylamine **11**.[57] These compounds were also tested in the LANCE*Ultra in vitro* demethylation assay (Table 1), revealing that **12a** with one phenol group retained some, albeit drastically reduced, inhibitory potency, while **12b** was completely inactive.

Encouraged by the finding that deferasirox **3a** is a JMJD2A *in vitro* inhibitor, we investigated its biological effects in a cell culture model using KYSE-150 esophageal cancer cells, known to be sensitive to KDM inhibition,[30] as well as in HL-60 leukemia cells. Deferasirox **3a** showed potent antiproliferative effects on both cell lines in an MTS assay with GI_{50} values in the single-digit micromolar range (Table 3). Importantly, the less polar uncharged derivatives **3b** and **3c** showed a 7-fold improvement relative to **3a** in KYSE-150 cells. Further, **3d** with lipophilic Cl substituents was still 4-fold more potent than **3a** despite the presence of a charged carboxylate. While HL-60 cells are generally less susceptible to growth inhibition than KYSE-150 cells, the observed trend in potency was the same. The differences in potency likely reflect, at least in part, improved cell permeability of the more hydrophobic derivatives **3b-d**. It cannot be ruled out that the ester compound **3c** is, at least in part, hydrolyzed by esterases in cells to the free carboxylic acid **3a** and, thus, rather functions as a prodrug of **3a**. However, as both **3a** and **3c** are virtually equipotent *in vitro*, the biological effect would be the same, once the compound has crossed the cell membrane.

Pleasingly, the control compound **12b** with no inhibitory activity (Table 1) also exhibited virtually no antiproliferative effect (Table 3).

Table 3. Antiproliferative effect of deferasirox-based inhibitors **3a-e** and control compound **12b** on KYSE-150 esophageal cancer and HL-60 leukemia cells.[a] n. i. – no inhibition.

Entry	KYSE-150 cells GI_{50} / μM	HL-60 cells GI_{50} / μM
3a	3.27 ± 0.62	5.5 ± 0.4
3b	0.45 ± 0.06	1.7 ± 0.3
3c	0.46 ± 0.06	1.7 ± 0.2
3d	0.85 ± 0.21	5.7 ± 1.3
3e	2.24 ± 0.06	7.4 ± 6.8
12b	17% inhib. @ 50 μM	n. i.

[a] Data are mean ± s. d. of triplicate experiments.

We then extended our analysis of the cellular effects of **3a** and its methyl ester **3c** to a broader panel of esophageal cancer cell lines, where we observed a potent growth inhibitory effect and consistently higher potency for the less polar compound **3c** (Supporting Figure 7).

Moreover, we extended our analysis to a panel of 18 lung adenocarcinoma cell lines and three non-transformed lung-derived cell lines (BEAS-2B, IMR-90, WI-38), which were treated either with **3a** or **3c**, the reference JmjC KDM inhibitor JIB-04[33, 46] or one of two inhibitors each of the histone demethylase LSD1 (KDM1A) and of histone deacetylases (HDACs). The full results of the screening of an epigenetic inhibitor library against the lung cancer cell line panel will be reported in due course elsewhere. For structures of the used inhibitors, refer to Supporting Figure 8a. For the majority of tumor cell lines, **3a** and **3c** led to loss of cell viability, with **3c** being significantly more potent at the same concentration (*t*-test: $p = 0.015$, Supporting

Figure 8b). Importantly, **3c** did not lead to loss of cell viability in all cell lines, arguing against non-specific cytotoxicity. This was especially apparent in two out of the three non-transformed cell lines: BEAS-2B and IMR-90. Comparative analysis revealed that the cellular response of **3c** on the entire panel of cell lines correlated best with that of parent compound **3a** and second best with the well-known JmjC KDM inhibitor JIB-04. This resemblance in biological activity again points to the specific action of **3a** and **3c** as *bona fide* JmjC KDM inhibitors within cells. On the other hand, there is little to no correlation to the biological activity profile of LSD1 or HDAC inhibitors (Figure 5).

		Compound 3a	Compound 3c	JIB-04	KK16	Vorinostat	AW84	JSF81
Compound 3a	JmJ inhibitor	1,00	0,97	0,98	0,09	0,08	0,03	0,07
Compound 3c	JmJ inhibitor	0,97	1,00	0,95	0,20	0,18	0,07	0,08
JIB-04	JmJ inhibitor	0,98	0,95	1,00	0,04	0,00	-0,09	-0,05
KK16	HDAC inhibitor	0,09	0,20	0,04	1,00	0,92	0,42	0,38
Vorinostat	HDAC inhibitor	0,08	0,18	0,00	0,92	1,00	0,55	0,54
AW84	LSD1 inhibitor	0,03	0,07	-0,09	0,42	0,55	1,00	0,92
JSF81	LSD1 inhibitor	0,07	0,08	-0,05	0,38	0,54	0,92	1,00

Figure 5. Heatmap of Pearson correlation coefficients for pairwise comparisons of inhibitor effects on cell viability on the panel of 18 tested lung adenocarcinoma cell lines. Chemical structures of and literature references to the used HDAC (KK16, Vorinostat) and LSD1 (AW84, JSF81) inhibitors can be found in Supporting Figure 8a.

Further support for on-target cellular KDM inhibition was observed in cells treated with **3a** as evidenced by a shift to overall increased masses of histones H3.1 and H3.2. This was shown by quantitative analysis of LC-MS data of histone proteins extracted from HEK293T cells treated with **3a** for 24 h, revealing a shift towards higher modification states (Supporting Figures 9-12). The corresponding immunoblots of histone extracts also manifested an increase in the levels of H3K4me$_3$, H3K9me$_3$, H3K27me$_3$, and H3K36me$_3$ methylation states upon treatment with **3a**, with no obvious changes in the levels of acetyl lysine (K-ac) (Figure 6a and Supporting Figure

13). This observation indicates an overall increase in histone H3 methylation, and methylation-specific action of **3a** rather than unspecific effects on chromatin (e.g. via changes in acetylation).

An increase in histone H3K9 trimethylation was also observed by immunofluorescence microscopy upon treatment of KYSE-150 cancer cells with **3a** and its synthetic derivatives **3b-e** (Figure 6b and Supporting Figure 14). Importantly, for the less polar derivatives **3b** and **3c**, lower concentrations were required to reach the same apparent level of increased trimethylation. Dose-dependent studies manifested an EC_{50} value of 40.5 μM for **3a**, 3.3 μM for **3b**, and 10 μM for **3c**, consistent with the improved antiproliferative effects of **3b**/**c** on cells (Table 3), likely caused by the enhanced cell permeability relative to **3a**. The potency of our compounds to upregulate histone trimethylation in the lower micromolar range is remarkable considering that other iron chelators such as deferiprone **2** and its derivatives only showed similar effects at concentrations of 100 or even up to 250 μM.[47]

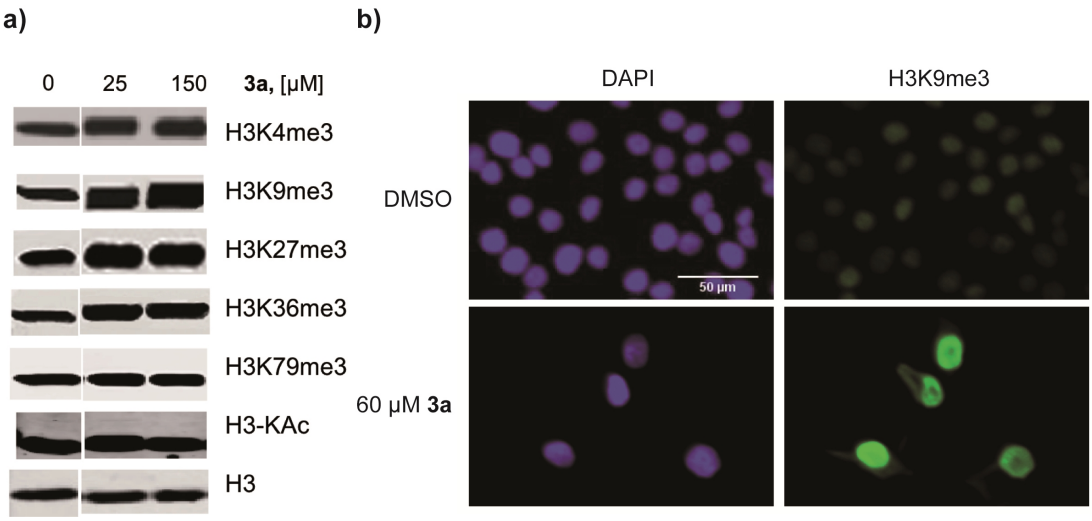

Figure 6. Treatment of cells with **3a** causes histone hypermethylation. a) Representative immunoblots of histone extracts from HEK293T cells treated with DMSO or **3a** for 24 h. b) Immunofluorescence microscopy of KYSE-150 cells treated with DMSO or **3a** for 72 h stained for H3K9 trimethylation.

Moreover, deferasirox and its analogues (**3a**-**c**) increased the H3K9me$_3$ staining in U2OS cells ectopically expressing JMJD2A in a concentration-dependent manner, suggesting that these compounds may quite directly inhibit demethylation by JMJD2A in cells. However, a dose-dependent increase in H3K9me$_3$ is also observed in cells overexpressing the catalytically inactive H188A variant of JMJD2A at higher concentrations (in particular **3c**), suggesting that these compounds may affect hypermethylation by also affecting endogenous KDMs or via other mechanisms. This is not unexpected as demonstrated by the promiscuity of KDM inhibition by **3a** *in vitro* (Table 2). Interestingly, consistent with the data obtained for the cell proliferation assays (Table 3), the cellular inhibition of JMJD2A was enhanced by an order of magnitude for the non-polar derivatives **3b** and **3c** relative to the more polar compounds (Figure 7 and Supporting Figure 15, Supporting Table 3).

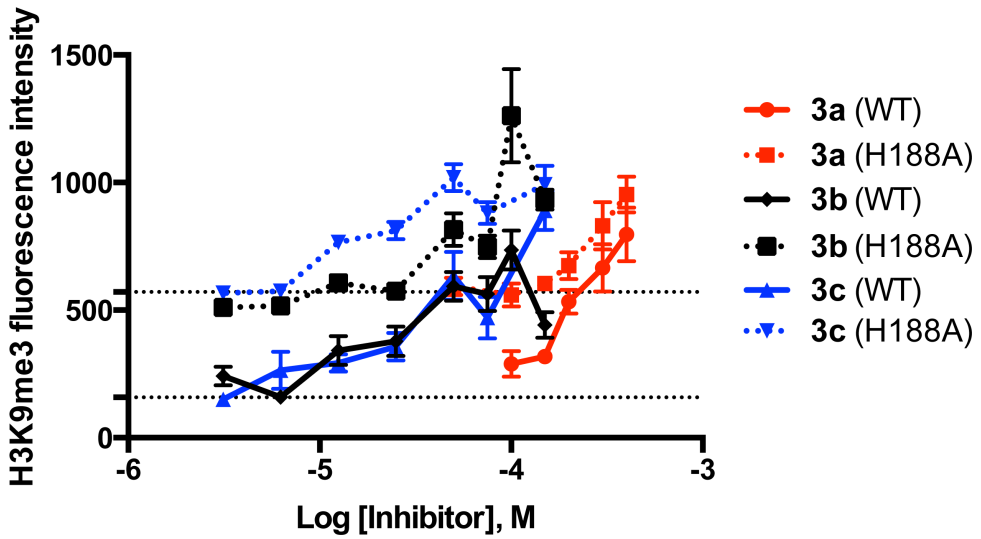

Figure 7. Quantitative immunofluorescence analysis of H3K9me$_3$ staining. U2OS cells overexpressing FLAG-KDM4A (wild type, WT) or catalytically inactive variant (H188A) were dosed with varying concentrations of **3a**, **3b**, or **3c** for 24 h. H3K9me$_3$ fluorescence intensities of KDM4A WT are shown as solid lines and H188A as dotted lines. On the intensity axis, the lower dashed grid line indicates the fluorescence intensity for control 1% DMSO dosed WT cells, whereas the upper dashed line indicates the control 1% DMSO dosed H188A cells. Shown is average fluorescence intensity (n > 50 cells ± s. e. m.).

We then investigated the generality of our results for human 2OG oxygenase inhibition (there are 60-70 such human enzymes). Because of its role in the regulation of erythropoietin (EPO), we studied the effects of **1** and **3a** on catalysis by the prolyl hydroxylase domain 2 (PHD2) enzyme, which is a 2OG oxygenase catalyzing hydroxylation of the hypoxia inducible factor-α subunits (HIF-α), using a peptide fragment of the C-terminal oxygen dependent degradation domain (CODD) of HIF-1α.[58] The results were similar to those observed for inhibition of JMJD2A. Thus, using a low concentration of Fe^{2+} in these inhibition assays, **1** and **3a** were moderately potent PHD2 inhibitors (2.4 ± 0.2 μM and 2.4 ± 0.2 μM, respectively), but at higher

Fe^{2+} concentration, the IC_{50} increased to 53.1 ± 12.5 μM with **3a** (Supporting Figure 16). NMR studies[58, 59] implied deferoxamine **1** inhibits substantially by Fe^{2+} sequestration in solution, whereas deferasirox **3a** inhibits by a mixture of protein binding and Fe^{2+} sequestration in solution. Interestingly, although protein binding has been observed under the NMR conditions, **3a** did not (efficiently) displace 2OG from PHD2.Zn complex or NOG from KDM4A.Fe complex, suggesting complexity in the inhibition modes (Supporting Figure 17). Note that metal ions are required for 2OG binding and the NMR results are compatible with the kinetic analyses due to the different conditions (i.e. the interaction of **1**/**3a** with the enzymes may be different under catalytic and non-catalytic conditions, due to conformational changes during catalysis). Consistent with prior reports,[60] both **1** and **3a** upregulated HIF-α levels in cells and inhibited ODD prolyl hydroxylation (Supporting Figure 18). Some histone-modifying enzymes are HIF target genes, thus, PHD inhibition by **1**, **3a**, and related compounds may account for some of the complexity in our cellular studies.

CONCLUSION. In summary, we have shown that the small molecule iron chelator deferasirox **3a** can function as a bona fide active site-binding small molecule inhibitor of Jumonji-type histone KDMs as evidenced by kinetic and extensive spectroscopic methods, both with isolated enzyme and in cancer cell lines. In contrast to deferoxamine **1**, which substantially inhibits by complexing Fe^{2+} in solution, as observed with JMJD2A and PHD2, **3a** has the potential to alter epigenetic regulation and gene expression by globally increasing histone methylation. The precise mode(s) of binding of **3a** to the JmjC KDMs, the PHDs, and potentially other 2OG oxygenases, requires further investigation. Our results imply more than one inhibition mode is likely involved. Deferasirox **3a** was developed to chelate iron ions in patient blood, so it

is highly soluble in water. Through simple chemical modifications, we have improved the biological effects of its core structure on intracellular targets, i.e. the JmjC KDMs. Deferasirox could, thus, be a starting point for the development of novel anticancer drugs based on a clinically proven lead structure and represents a valuable test compound to investigate the cellular effects of pan-KDM inhibition *in vitro* and, possibly, *in vivo*.

Indeed, there is already some evidence for a beneficial *in vivo* effect when cancer cells or patients have been treated with **3a**.[56, 61-65] Treatment with **1** or **3a** has been reported to inhibit proliferation of esophageal cancer cells in cell culture and a mouse xenograft model and increased susceptibility to standard chemotherapy. The mechanism of action, however, was elusive.[61] Similar effects were also observed for **3a** in leukemia cell lines, independent of exogenously supplied iron,[63] and gastric cancer cells.[64] In terms of clinical use, it was found that the mortality of patients with myelodysplastic syndromes receiving frequent blood transfusions was significantly reduced when they were additionally treated with **3a**.[65, 66] Therefore, the use of iron chelators like **3a** has been proposed as a novel avenue in antitumor treatment.[67-69]

Our results suggest that the observed anticancer potential may be due, at least in part, to 2OG oxygenase inhibition and the consequent changes in epigenetic gene regulation of cancer cells. As much pharmacological and clinical safety data for this compound class are already available, **3a** is an attractive starting point for further development. Our results, however, also raise concerns because **3a** is currently in clinical use for an entirely unrelated disorder (iron overload disease) and the potential epigenetic effects of this compound due to the modulation of histone methylation and hence, transcription, might have been overlooked so far.

EXPERIMENTAL SECTION

Test compounds

Clinically used iron chelators were from commercial sources and used for testing without further purification. Deferoxamine mesylate **1** was from Sigma-Aldrich (catalog: D9533), deferiprone **2** was from Acros Organics (catalog: 278740050), and deferasirox **3a** was obtained from Selleckchem (catalog: S1712) for the initial *in vitro* screening and from AK Scientific (catalog: V0697) for the mass spectrometric analyses. Later, it was re-synthesized in house (see below) and the results confirmed those obtained with the commercial sample. Derivatives **3b**-**f** were synthesized in house (see below).

All screening compounds **1**, **2**, **3a**-**f**, **12a**/**b** were tested for known classes of assay interference compounds using the publicly available online tool "False Positive Remover" (www.cbligand.org/PAINS). None of the tested compounds were flagged as PAINS. Moreover, all compounds reported in this study were characterized in at least two *in vitro* assays with different readout techniques to provide orthogonal proof of their specific activities.

Enzyme inhibition assays were performed as previously reported.[21-23]

JMJD2A (KDM4A) FDH assay: The formaldehyde dehydrogenase (FDH) enzyme-coupled demethylase activity assay was performed in a total volume of 20 µL on white OptiPlate-384 microtiter plates (PerkinElmer) using a 50 mM HEPES buffer at pH = 7.50 containing 0.01% (v/v) Tween-20. A solution of 0.10 $mg \cdot mL^{-1}$ (2.4 µM) KDM4A 1-359 was pre-incubated with compound solutions of varying concentration (0 – 400 µM) in DMSO at room temperature for 10 minutes. A substrate solution containing 100 µM ascorbic acid, 10 µM $FeSO_4$, 0.001 $U \cdot \mu L^{-1}$ FDH, 500 µM NAD^+, 50 µM 2-oxoglutarate, and 35 µM of H3K9me_3 7-14 substrate peptide ARK(me_3)-STGGK-NH_2 (PSL Peptide Specialty Laboratories) was added (final concentrations).

Final DMSO concentration was 2% (v/v) in all wells. Fluorescence intensity of the forming product NADH was measured at λ_{ex} = 330 nm and λ_{em} = 460 nm on a POLARstar Optima microplate reader (BMG Labtech) immediately after addition (t = 0) and after one hour of incubation on a horizontal shaker at 37°C. Values were blank-corrected and the difference in intensity at t = 1 h and t = 0 was taken as a measurement of enzyme activity. Activity in % is in comparison to compound-free DMSO control and no-substrate negative control. Inhibition curves were analyzed by sigmoidal curve fitting using GraphPad Prism 4.00 and IC_{50} values calculated from the fit parameters as mean ± s. d. from two independent experiments.

JMJD2A (KDM4A) LANCE assay: The commercial antibody-based LANCE*Ultra* demethylase activity assay (PerkinElmer) was performed in a total volume of 10 µL on white OptiPlate-384 microtiter plates (PerkinElmer) using a 50 mM HEPES buffer at pH = 7.50 containing 0.01% (v/v) Tween-20 and 0.01% (w/v) BSA. A solution of 60 nM JMJD2A (KDM4A) 1-359 was pre-incubated with compound solutions of varying concentration in DMSO at room temperature for 10 minutes. A substrate solution containing 100 µM ascorbic acid, 5 µM $FeSO_4$, 1 µM 2-oxoglutarate, and 400 nM of biotinylated H3K9me_3 1-21 substrate peptide ARTKQTARK(me_3)-STGGKAPRKQLA-GGK(biotin) (BPS Bioscience) was added (final concentrations). Final DMSO concentration was 5% (v/v) in all wells. Plates were incubated on a horizontal shaker at room temperature for 45 minutes. Reactions were stopped by addition of 10 µL of detection mix containing 2 nM europium-labeled anti-H3K9me_2 LANCE antibody (PerkinElmer), 50 nM U*Light*-streptavidin dye (PerkinElmer), and 1 mM EDTA in 1X LANCE detection buffer (PerkinElmer) (final concentrations). Plates were again incubated on a horizontal shaker at room temperature for 60 minutes. FRET intensity was measured on a PerkinElmer EnVision 2102 multilabel plate reader at λ_{ex} = 340 nm and λ_{em} = 665 nm with a

delay of 100 µs. Values were blank-corrected and activity in % is in comparison to compound-free DMSO control and no-enzyme negative control. Inhibition curves were analyzed by sigmoidal curve fitting using GraphPad Prism 4.00 (GraphPad Software) and IC_{50} values calculated from the fit parameters as mean ± s. d. from two independent experiments.

JARID1A (KDM5A) LANCE assay: The antibody-based LANCE*Ultra* activity assay for JARID1A (KDM5A) was performed essentially as described for JMJD2A (KDM4A) with the following modifications: a solution of 25 nM full-length JARID1A 1-1090 (BPS BioScience) was used with 100 nM of biotinylated H3K4me_3 1-21 substrate peptide ARTK(me_3)-QTARKSTGGKAPRKQLA-GGK(biotin) (AnaSpec). The detection mix contained the appropriate europium-labeled anti-H3K4me_2/me_1 LANCE antibody (PerkinElmer).

JMJD3 (KDM6B) LANCE assay: The antibody-based LANCE*Ultra* activity assay for JMJD3 (KDM6B) was performed essentially as described for JMJD2A (KDM4A) with the following modifications: a solution of 50 nM catalytic domain JMJD3 1043-end (BPS BioScience) was used with 400 nM of biotinylated H3K27me_3 21-44 substrate peptide ATKAARK(me_3)-SAPATGGVKKPHRYRPG-GK(biotin) (PSL Peptide Specialty Laboratories). Incubation time for the enzymatic reaction was 120 min and the detection mix contained the appropriate europium-labeled anti-H3K27me_2 LANCE antibody (PerkinElmer).

JMJD2A (KDM4A) 2-oxoglutarate competition assay: In order to assess the competitivity of enzyme inhibition by test compounds to 2-oxoglutarate, the LANCE*Ultra* assay was performed as described above with varying concentrations of 2-oxoglutarate (0 – 5.0 µM) and inhibitor. Each combination was tested in duplicate. The blank-corrected LANCE signal was compared to a pre-established calibration curve to determine the amount of demethylated product formed and, thus, the reaction velocity over the incubation time. Curve fitting for compounds that were not

competitive with regard to 2-oxoglutarate (Supporting Figure 2) was performed using the Michaelis-Menten equation:

$$v = \frac{v_{max} \cdot [\text{2-oxoglutarate}]}{K_M + [\text{2-oxoglutarate}]}.$$

EPR spectroscopy

All Q-band electron paramagnetic resonance (EPR) measurements were performed on a Bruker ELEXSYS E580 spectrometer equipped using a Bruker EN 5107D2 1.6 mm dielectric resonator. Temperature (4 K) was controlled by a liquid helium cryostat (Oxford CF935O) and an ITC temperature controller (Oxford ITC4). Field-sweep echo detected EPR spectra were recorded at a magnetic field range of 0 – 1400 mT using a $\pi/2$ pulse of 16 ns and a τ value of 32 ns at 6 dB microwave power. All obtained spectra were pseudo-modulated (14 mT modulation amplitude) after subtraction of a linear background function.

Three-pulse ESEEM data were collected using a $\pi/2 - \tau - \pi/2 - \tau - \pi/2$ pulse sequence ($\pi/2$ = 16 ns; τ = 100 ns) together with a four-step phase cycling. Primary ESEEM data were further processed by subtraction of an exponential decay background function, processed by a Hamming window, zero-filled to 1500 points, and Fourier-transformed.

All samples contained 100 μM $FeSO_4$. Enzyme-containing samples contained 65 μM of the catalytic domain of JMJD2A residues 1-359. Deferasirox **3a** concentrations were variable from 0, 25, 50, 100, 150, to 200 μM. For the sample without enzyme, [3a] was 200 μM.

In contrast to enzyme activity or kinetic experiments, these samples did not contain any ascorbic acid as reducing agent so that a partial oxidation from Fe^{2+} to Fe^{3+} was possible. Therefore, iron(III) species are observed in all EPR spectra.

NMR spectroscopy

All nuclear magnetic resonance (NMR) spectra were recorded with a Bruker AVIII 600 MHz NMR spectrometer equipped with a BB-F/1H Prodigy N_2 cryoprobe using 3 mm diameter tubes (Norell). Data were processed with Bruker 3.1 software.

Assay mixtures were buffered in 50 mM Tris-d_{11}, pH 7.5, in 10% D_2O and 90% H_2O containing 50 μM Zn^{2+} (except for KDM4A experiments, the enzyme was in its Fe^{2+}-metallated state).

^{1}H excitation sculpting suppression NMR: Spectra were typically obtained using 256 scans and a relaxation delay of 1 s. A 2 ms Sinc pulse was used for water suppression. Prior to Fourier transformation, data were multiplied with an exponential function with 2 Hz line broadening.[58]

^{1}H CPMG NMR: Typical experimental parameters for Carr-Purcell-Meiboom-Gill (CPMG) NMR spectroscopy were: total echo time: 40 ms; relaxation delay: 2 s; and number of transients: 264. The PROJECT-CPMG sequence ($90° x – [\tau – 180° y – \tau – 90° y – \tau – 180° y – \tau]_n$ – acq) was applied. Water suppression was achieved by presaturation. Prior to Fourier transformation, the data were multiplied with an exponential function with 3 Hz line broadening.[58]

wLOGSY NMR experiments: water-Ligand Observed Gradient SpectroscopY (wLOGSY) experiments were conducted using the pulse sequence described by Dalvit et al.[70] Typical experimental parameters were as follows: mixing time: 1 s; relaxation delay: 2 s; and number of transients: 256. Solvent excitation was achieved using a 16 ms 180° selective rectangular shape pulse with 1000 points (Squa100.1000) set at the H_2O frequency. Water suppression was achieved by a 2 ms Sinc pulse (Sinc1.1000) at the H_2O frequency.[58]

Immunoblotting

Histones were prepared as described above by acid extraction from HEK293T cells. Approximately 0.2 µg of extracted proteins were separated by SDS-PAGE and analyzed by immunoblotting with antibodies directed against H3 (abcam, ab10799), H3K9me$_3$ (abcam, ab8898), H3K36me$_3$ (abcam, ab9050), H3K79me$_3$ (abcam, ab2621), acetyl-lysine (abcam, ab61257), and H3K27me$_3$ (Merck Millipore, 07-449) to investigate changes in specific histone modifications. Immunoblots were imaged using fluorescent secondary antibodies and Odyssey infrared imaging technology (LI-COR Biosciences), enabling quantification of histone marks by infrared fluorescent signals, which are directly proportional to the amount of antigen.

Immunofluorescence microscopy in KYSE-150 cells

4,000 cells per well were cultured overnight in sterile ViewPlate-96 black culture plates (PerkinElmer) at 37°C and 5% CO_2. Compounds were added to a final concentration of 1.0 – 100 µM in 0.5% DMSO and incubated for 72 h at 37°C and 5% CO_2. The following work was performed at room temperature. Cells were washed with phosphate-buffered saline (PBS), fixed for 20 minutes with 4% formaldehyde in PBS, and washed with PBS. After cells were permeabilized with 0.5% Triton X-100 in PBS for 8 minutes, non-specific binding sites were blocked with 3% FCS in PBS for 30 minutes. Cells were incubated with the 1:500 diluted primary antibody rabbit anti-H3K9me$_3$ (abcam, ab8898) in 3% FCS in PBS overnight. After washing three times with PBS, the secondary antibody anti-rabbit Alexa Fluor® 488 (Life Technologies, A-11008) was added in a 1:500 dilution in 3% FCS in PBS and incubated for 1 h in the dark. After a threefold washing step with PBS, cells were stained with DAPI (10 µg·mL^{-1}

in PBS) for 5 minutes. Image acquisition was conducted in PBS, after a threefold washing step with PBS, using an Olympus Scan^R Screening station.

Immunofluorescence microscopy in U2OS cells with wild-type and mutant KDM4A

U2OS cells were maintained in 10% FBS, 1 mM glutamine in DMEM at 37°C and 5% CO_2. Cells were seeded at 500 cells per well in black CellCarrier-96 plates (PerkinElmer) and incubated overnight. Cells were transfected with pCDNA3-FLAG-KDM4A (WT) or catalytically inactive control pCDNA3-FLAG-KDM4A H188A (MUT)[71] using Lipofectamine 3000 (Thermo) in OPTIMEM. After 4 h, the transfection reagent was replaced with media supplemented with inhibitors (1% (v/v) DMSO final) and incubated for further 24 h. Cells were washed with PBS, fixed and permeabilized, and stained as previously described.[26] Cells were stained for FLAG (mouse monoclonal, Sigma, F1804), H3K9me_3 (rabbit polyclonal, abcam, ab8898) and DAPI (Sigma, D9564) and probed using fluorescence-conjugated secondary antibodies (goat anti-rabbit Alexa Fluor 488, Life Technologies, A11034 and goat anti-mouse Alexa Fluor 594, Life Technologies, A11032). Image acquisition was performed using an Operetta high content imaging system (PerkinElmer), and images were analyzed using Harmony software (PerkinElmer). Cell nuclei were automatically identified by DAPI staining. H3K9me_3 levels of cells overexpressing KDM4A WT/MUT were analyzed.

CHEMISTRY

General Methods. Starting materials, reagents, and analytical-grade solvents were obtained from commercial sources and used without further purification. Solvents for preparative chromatography were generally purified by distillation prior to use. Reaction progress was

monitored by analytical thin-layer chromatography (TLC) on pre-coated silica gel plates with fluorescence indicator (Merck silica gel 60 F_{254}) and spots were detected by UV light (λ = 254 nm or 365 nm). Flash column chromatography using gradient elution was performed using a Biotage IsoleraOne system with pre-packed Biotage SNAP cartridges or on manually packed column cartridges using Merck silica (particle size 40 – 63 μm) as indicated. ^{1}H-NMR and proton-decoupled ^{13}C-NMR spectra were recorded in the indicated deuterated solvents using a Bruker Avance DRX or Bruker III HD 400 MHz spectrometer. Chemical shifts (δ) are expressed in parts per million (ppm) and coupling constants (*J*) in Hz. Chemical shifts are normalized to the expected chemical shift of the residual solvent signal, i. e. ^{1}H δ = 2.50 and ^{13}C δ = 39.52 for DMSO-d_6 and ^{1}H δ = 7.26 and ^{13}C δ = 77.16 for $CDCl_3$, respectively. The following abbreviations are used: br s (broad singlet), s (singlet), d (doublet), dd (doublet of doublets), ddd (doublet of doublets of doublets), t (triplet), m (multiplet). Mass spectra were recorded using electrospray ionization (ESI-MS) or chemical ionization at atmospheric pressure (APCI-MS) using a Thermo Electron LCQ Advantage or Thermo Scientific Exactive mass spectrometer in positive and/or negative ion mode as indicated. The purity of the final compounds was determined by HPLC with UV detection at 210 nm. HPLC analysis was performed using an Agilent Technologies 1260 Infinity system, using a Phenomenex Synergi 4μ Hydro-RP 80 Å column (250 mm × 4.60 mm). Elution was performed at 30°C under gradient conditions. Eluent A was water containing 0.05% (v/v) trifluoroacetic acid (TFA). Eluent B was acetonitrile, also containing 0.05% (v/v) TFA. Linear gradient conditions were as follows: 0-4 min: A = 90%, B = 10%; 4-29 min: linear increase to B = 100%; 29-31 min: B = 100%; 31-40 min: A = 10%, B = 90%. A flow rate of 1 mL·min^{-1} was maintained. Melting points were recorded on a Stuart Scientific SMP2 melting point apparatus.

2-(2-Hydroxyphenyl)-4H-1,3-benzoxazin-4-one (6a). According to a reported procedure,[53] 2.00 g (14.6 mmol, 1.0 eq) salicylamide **4a** and 2.42 g (17.5 mmol, 1.2 eq) salicylic acid **5a** were suspended in 3.00 mL of xylenes (mixture of isomers). 146 µL dry pyridine was added and the mixture was brought to reflux, where it became a clear golden solution. 2.33 mL (3.82 g, 32.1 mmol, 2.2 eq) of thionyl chloride was added dropwise over 2 hours. An intense evolution of gases was observed after each addition and the solution became much darker. Upon completion of the addition, a yellowish solid material started to precipitate from the then viscous brown solution. Heating was discontinued and the mixture stirred for another 30 min. Volatiles were removed *in vacuo* and the remaining yellow solid material resuspended in 8.80 mL ethanol and 146 µL glacial acetic acid. The mixture was brought to reflux and cooled. The crystalline yellow solid was collected by suction filtration, washed with cold ethanol and dried *in vacuo* to yield the desired product. When exposed to moisture, the product slowly decomposes to bis(salicyl)imide. ^{1}H-NMR spectra in DMSO-d_6 containing traces of water show both products. Yield, 72% of a yellow powder; M. p.: 208°C; ^{1}H-NMR (400 MHz, $CDCl_3$, δ [ppm]): 12.70 (br s, 1H), 8.19 (dd, J = 8.1 Hz, 1.7 Hz, 1H), 8.09 (dd, J = 8.1 Hz, 1.7 Hz, 1H), 7.79 (ddd, J = 8.5 Hz, 7.3 Hz, 1.7 Hz, 1H), 7.58–7.45 (m, 3H), 7.06 (dd, J = 8.5 Hz, 1.1 Hz, 1H), 6.98 (ddd, J = 8.2 Hz, 7.3 Hz, 1.1 Hz, 1H). ^{13}C-NMR (101 MHz, $CDCl_3$, δ [ppm]): 165.2, 164.0, 163.2, 154.2, 136.9, 135.7, 128.7, 128.0, 127.3, 119.5, 118.9, 118.3, 117.0, 111.3.

6-Chloro-2-(5-chloro-2-hydroxyphenyl)-4H-1,3-benzoxazin-4-one (6d). As a variation of a reported procedure,[53] 2.00 g (11.7 mmol, 1.0 eq) 5-chlorosalicylamide **4d** and 2.41 g (14.0 mmol, 1.2 eq) 5-chlorosalicylic acid **5d** were suspended in 12.4 mL of xylenes (mixture of isomers). 720 µL dry pyridine was added and the mixture was brought to reflux. 1.86 mL (3.05 g, 25.6 mmol, 2.2 eq) of thionyl chloride was added dropwise over 2 hours, during which

time the mixture became a clear solution. An intense evolution of gases was observed after each addition and the solution became much darker. Upon completion of the addition, a white solid material started to precipitate from the viscous mixture. The mixture was cooled to room temperature and volatiles were removed *in vacuo*. The remaining pale yellow solid material was resuspended in 10.0 mL ethanol and 120 µL glacial acetic acid. The mixture was brought to reflux and cooled. The crystalline solid was collected by suction filtration, washed with cold ethanol, and dried *in vacuo* yielding the desired product. Yield, 55% of a pale yellow powder; M. p., 260°C; ^{1}H-NMR (400 MHz, $CDCl_3$, δ [ppm]): 12.52 (br s, 1H), 8.18 (d, J = 2.6 Hz, 1H), 8.04 (d, J = 2.7 Hz, 1H), 7.77 (dd, J = 8.9 Hz, 2.6 Hz, 1H), 7.52 (d, J = 8.9 Hz, 1H), 7.49 (dd, J = 9.0 Hz, 2.7 Hz, 1H), 7.06 (d, J = 9.0 Hz, 1H). ^{13}C-NMR (101 MHz, $CDCl_3$, δ [ppm]): 164.2, 162.6, 161.8, 152.4, 137.1, 136.2, 133.4, 127.7, 127.6, 124.6, 120.7, 119.3, 118.8, 111.8. HPLC: t_R = 24.96 min, 99% purity.

2-(2-Hydroxy-5-methoxyphenyl)-6-methoxy-4*H*-1,3-benzoxazin-4-one (6e). As a variation of a reported procedure,[53] 900 mg (5.38 mmol, 1.0 eq) 5-methoxysalicylamide **4e** and 1.09 g (6.46 mmol, 1.2 eq) 5-methoxysalicylic acid **5e** were suspended in 2.20 mL of xylenes (mixture of isomers). 60.0 µL dry pyridine was added and the mixture was brought to reflux, where it became a clear orange solution. Under vigorous stirring, 860 µL (1.41 g, 11.8 mmol, 2.2 eq) of thionyl chloride was added dropwise over 1.5 hours. An intense evolution of gases was observed after each addition and the solution became much darker. Upon completion of the addition, a solid material started to precipitate from the viscous dark mixture. The mixture was refluxed for another 30 min, cooled to room temperature, then volatiles were removed *in vacuo*. The remaining brown oil was resuspended in 5.00 mL ethanol and 60.0 µL glacial acetic acid. The mixture was brought to reflux, cooled, and precipitation completed in an ice bath for one hour.

The brown solid material was collected by suction filtration, washed with cold ethanol, and dried *in vacuo* yielding the desired product. Yield, 39% of a brown powder; M. p.: 206°C (decomp.); ^{1}H-NMR (400 MHz, $CDCl_3$, δ [ppm]): 12.26 (br s, 1H), 7.54 (d, J = 3.0 Hz, 1H), 7.48–7.42 (m, 2H), 7.34 (dd, J = 9.1 Hz, 3.0 Hz, 1H), 7.14 (dd, J = 9.1 Hz, 3.1 Hz, 1H), 7.00 (d, J = 9.1 Hz, 1H), 3.91 (s, 3H), 3.85 (s, 3H). ^{13}C-NMR (101 MHz, $CDCl_3$, δ [ppm]): 164.7, 164.3, 158.3, 157.8, 152.3, 148.7, 125.2, 125.2, 119.9, 118.9, 118.5, 110.8, 110.4, 107.6, 56.2, 56.1.

5-Fluoro-*N*-(5-fluoro-2-hydroxybenzoyl)-2-hydroxybenzamide (8). As a variation of a reported procedure,[53] 594 mg (3.83 mmol, 1.0 eq) 5-fluorosalicylamide **4f** and 658 mg (4.21 mmol, 1.1 eq) 5-fluorosalicylic acid **5f** were suspended in 6.54 mL of xylenes (mixture of isomers). 31.0 µL of dry pyridine was added and the mixture was brought to reflux. Under vigorous stirring, 583 µL (957 mg, 8.04 mmol, 2.1 eq) of thionyl chloride was added dropwise over 2 hours. An intense evolution of gases was observed after each addition and the color changed from yellow to red. The mixture was refluxed for additional 60 min, cooled to room temperature, then volatiles were removed *in vacuo*. The remaining dark red residue was resuspended in 4.00 mL of methanol and 30.0 µL glacial acetic acid. The mixture was brought to reflux. The insoluble solid material was collected by suction filtration, washed with hot methanol, and dried *in vacuo* yielding the desired product. Yield, 32% of a light brown powder; M. p.: 202°C (decomp.); ^{1}H-NMR (400 MHz, DMSO-d_6, δ [ppm]): 12.07 (br s, 1H), 11.35 (br s, 2H), 7.55 (dd, J = 9.5, 3.3 Hz, 2H), 7.39–7.28 (m, 2H), 7.05 (dd, J = 9.0, 4.5 Hz, 2H). ^{13}C-NMR (101 MHz, DMSO-d_6, δ [ppm]): 163.43 (d, J = 2.2 Hz), 155.62 (d, J = 235.5 Hz), 153.38 (d, J = 1.2 Hz), 121.56 (d, J = 23.5 Hz), 120.31 (d, J = 6.5 Hz), 119.04 (d, J = 7.5 Hz), 116.49 (d, J = 24.4 Hz). ^{19}F-NMR (376 MHz, DMSO-d_6, δ [ppm]): -124.25 – -124.39 (m, 2F). ESI-MS (+,

MeOH): 294.0570 $[M+H]^+$, 316.0388 $[M+Na]^+$. Calcd. for $[C_{14}H_9F_2NO_4+H]^+$: 294.0572. ESI-MS (–, MeOH): 292.0427 $[M–H]^–$. Calcd. for $[C_{14}H_9F_2NO_4-H]^–$: 292.0427.

Methyl 4-hydrazinylbenzoate (7c). According to a reported procedure,[55] 10.0 g (65.7 mmol, 1.0 eq) of 4-hydrazinylbenzoic acid **7a** was suspended in 300 mL methanol. 3.50 mL (6.45 g, 65.7 mmol, 1.0 eq) concentrated sulfuric acid were added dropwise, leading to an intensification of the reddish color. The mixture was brought to reflux, where it became a clear reddish solution, then stirred at reflux overnight. After 18 h, stirring was suspended, the mixture cooled, and volatiles were removed *in vacuo*. The resultant brown powder was resuspended in 700 mL dichloromethane, neutralized by the addition of 300 mL saturated $NaHCO_3$ solution and the organic phase washed with another 2x 150 mL $NaHCO_3$ solution and once with 150 mL brine. The organic phase was dried over Na_2SO_4, filtered, and volatiles were removed *in vacuo*, to give the desired product. Yield, 36% of an orange powder; M. p.: 109°C; ^{1}H-NMR (400 MHz, DMSO-d_6, δ [ppm]): 7.69 (d, J = 8.8 Hz, 2H), 7.56 (br s, 1H), 6.76 (d, J = 8.8 Hz, 2H), 4.18 (br s, 2H), 3.73 (s, 3H). ^{13}C-NMR (101 MHz, DMSO-d_6, δ [ppm]): 166.5, 156.1, 130.8, 116.2, 109.9, 51.2.

4-[3,5-Bis(2-hydroxyphenyl)-1*H*-1,2,4-triazol-1-yl]benzoic acid (3a). According to a reported procedure,[52] 1.00 g (4.18 mmol, 1.0 eq) 2-(2-hydroxyphenyl)-4*H*-1,3-benzoxazin-4-one **6a** and 700 mg (4.60 mmol, 1.1 eq) 4-hydrazinylbenzoic acid **7a** were suspended in 15.0 mL of methanol. The mixture was brought to reflux, where it became a clear orange solution. After ca. 45 min, the mixture became turbid and stirring was stopped after 2 hours. Upon cooling, larger amounts of white solid formed, whose precipitation was completed in an ice bath. The off-white solid was collected by suction filtration and the raw material recrystallized from 65 mL of methanol, yielding the desired product. Yield, 46% of pale brown crystals; M. p.: 266°C; ^{1}H-

NMR (400 MHz, DMSO-d_6, δ [ppm]): 13.21 (br s, 1H), 10.81 (s, 1H), 10.06 (s, 1H), 8.05 (dd, J = 7.8 Hz, 1.6 Hz, 1H), 8.02–7.96 (m, 2H), 7.59–7.53 (m, 3H), 7.43–7.34 (m, 2H), 7.06–6.95 (m, 3H), 6.86 (d, J = 8.2 Hz, 1H). ^{13}C-NMR (101 MHz, DMSO-d_6, δ [ppm]): 166.5, 159.9, 156.4, 155.2, 152.1, 141.2, 132.6, 131.5, 131.1, 130.6, 130.3, 126.8, 123.4, 119.7, 119.5, 117.1, 116.2, 114.4, 113.7. ESI-MS(+, MeOH): 374.1137 $[M+H]^+$. Calcd. for $[C_{21}H_{15}N_3O_4+H]^+$: 374.1135. ESI-MS(–, MeOH): 372.0993 $[M–H]^–$, 328.1094 $[M–CO_2–H]^–$. Calcd. for $[C_{21}H_{15}N_3O_4–H]^–$: 372.0990. HPLC: t_R = 21.75 min, 98% purity.

2,2'-(1-Phenyl-1*H*-1,2,4-triazole-3,5-diyl)diphenol (3b). According to a reported procedure,[53] 145 mg (1.00 mmol, 1.2 eq) phenylhydrazine hydrochloride **7b** were suspended in 8.00 mL of ethanol and brought to reflux, to give a pale yellow solution. To this were added 200 mg (0.836 mmol, 1.0 eq) 2-(2-hydroxyphenyl)-4*H*-1,3-benzoxazin-4-one **6a** and the mixture stirred at reflux for 2.5 hours. After cooling to room temperature, ~10 mL of 1 mol·L^{-1} hydrochloric acid were added dropwise, resulting in the formation of a white precipitate, which was filtered off, washed with more 1 mol·L^{-1} HCl and dried *in vacuo* yielding the desired product. Yield, 56% of a white powder; M. p.: 155°C; ^{1}H-NMR (400 MHz, DMSO-d_6, δ [ppm]): 10.89 (s, 1H), 10.06 (s, 1H), 8.04 (dd, J = 7.8 Hz, 1.7 Hz, 1H), 7.50–7.41 (m, 6H), 7.40–7.32 (m, 2H), 7.05–6.97 (m, 2H), 6.94 (ddd, J = 7.5 Hz, 7.5 Hz, 1.0 Hz, 1H), 6.87 (dd, J = 8.3 Hz, 0.8 Hz, 1H). ^{13}C-NMR (101 MHz, DMSO-d_6, δ [ppm]): 159.5, 156.3, 155.4, 151.7, 137.7, 132.3, 131.3, 131.0, 129.2, 128.6, 126.6, 123.8, 119.6, 119.2, 117.0, 116.1, 114.6, 113.8. APCI-MS (+, MeOH): 330.1230 $[M+H]^+$. Calcd. for $[C_{20}H_{15}N_3O_2+H]^+$: 330.1237. APCI-MS (–, MeOH): 328.1092 $[M–H]^–$. Calcd. for $[C_{20}H_{15}N_3O_2–H]^–$: 328.1092. HPLC: t_R = 22.94 min, 97% purity.

Methyl 4-[3,5-bis(2-hydroxyphenyl)-1*H*-1,2,4-triazol-1-yl]benzoate (3c). According to a reported procedure,[54] 3.00 g (12.5 mmol, 1.0 eq) 2-(2-hydroxyphenyl)-4*H*-1,3-benzoxazin-4-one

6a and 2.29 g (13.8 mmol, 1.1 eq) methyl 4-hydrazinylbenzoate **7c** were suspended in 200 mL of ethanol. 1.77 mL (1.29 g, 12.8 mmol, 1.02 eq) triethylamine were added dropwise. The mixture was brought to reflux, when it became a clear orange solution. After 2.5 hours, heating was stopped and stirring was continued for another hour. The mixture was diluted with 300 mL distilled water, when a white precipitate formed. The mixture was concentrated to about half its volume *in vacuo* and acidified by the addition of ~10 mL glacial acetic acid. 300 mL dichloromethane were added and the phases separated. The aqueous phase was extracted with further 3x 150 mL dichloromethane. The combined organic layers were dried over Na_2SO_4, filtered, and freed from all volatiles *in vacuo*. The remaining orange powder was further purified by column chromatography (100 g silica gel, manually packed Biotage cartridge using dry load sorbent, dichloromethane/methanol 100:0% → 99:1% (v/v)), yielding the desired product. Yield, 58% of a pale yellow powder; M. p.: 178°C; ^{1}H-NMR (400 MHz, $CDCl_3$, δ [ppm]): 11.28 (br s, 1H), 9.59 (br s, 1H), 8.27–8.21 (m, 2H), 8.17–8.10 (m, 1H), 7.64–7.58 (m, 2H), 7.42–7.31 (m, 2H), 7.18–7.12 (m, 1H), 7.11–7.00 (m, 2H), 6.92 (dd, J = 8.0 Hz, 1.6 Hz, 1H), 6.71–6.62 (m, 1H), 4.00 (s, 3H). ^{13}C-NMR (101 MHz, $CDCl_3$, δ [ppm]): 165.9, 159.6, 158.1, 156.6, 152.2, 141.6, 133.3, 132.1, 131.8, 131.4, 127.8, 127.7, 126.2, 120.1, 119.2, 118.6, 117.3, 113.1, 109.9, 52.8. ESI-MS (+, MeOH): 388.1292 $[M+H]^+$, 410.1111 $[M+Na]^+$. Calcd. for $[C_{22}H_{17}N_3O_4+H]^+$: 388.1292. ESI-MS (–, MeOH): 386.1150 $[M–H]^–$. Calcd. for $[C_{22}H_{17}N_3O_4–H]^–$: 386.1146. HPLC: t_R = 25.39 min, 98% purity.

4-[3,5-Bis(5-chloro-2-hydroxyphenyl)-1*H*-1,2,4-triazol-1-yl]benzoic acid (3d). In a variation of the reported procedure,[52] 700 mg (2.27 mmol, 1.0 eq) 6-chloro-2-(5-chloro-2-hydroxyphenyl)-4*H*-1,3-benzoxazin-4-one **6d** and 380 mg (2.50 mmol, 1.1 eq) 4-hydrazinylbenzoic acid **7a** were suspended in 52.4 mL of methanol. The mixture was brought to reflux, where it became a clear

orange solution over time. After 4.5 hours, stirring was stopped and the mixture cooled to room temperature, when large amounts of white solid material formed, whose precipitation was completed in an ice bath. The material was collected by suction filtration and dried; ^{1}H-NMR spectral analysis identified this material as the starting material **6d**. The mother liquor was left standing in a refrigerator for three days until another white solid crystallized, which was collected by suction filtration, dried *in vacuo*, and identified as the desired product. Yield, 25% of a white powder; M. p.: 268°C; ^{1}H-NMR (400 MHz, DMSO-d_6, δ [ppm]): 13.23 (br s, 1H), 10.67 (s, 1H), 10.37 (s, 1H), 8.04–7.99 (m, 2H), 7.99 (d, J = 2.7 Hz, 1H), 7.67 (d, J = 2.7 Hz, 1H), 7.62–7.55 (m, 2H), 7.47–7.38 (m, 2H), 7.08 (d, J = 8.8 Hz, 1H), 6.86 (d, J = 8.8 Hz, 1H). ^{13}C-NMR (101 MHz, DMSO-d_6, δ [ppm]): 166.5, 158.8, 155.0, 154.2, 151.0, 141.0, 132.4, 131.1, 130.8, 130.5, 130.4, 126.1, 123.4, 123.3, 122.8, 119.2, 117.9, 116.0, 115.4. ESI-MS (+, MeOH): 442.03558, 444.03265, 446.02954 $[M+H]^+$. Calcd. for $[C_{21}H_{13}Cl_2N_3O_4+H]^+$: 442.03559, 444.03264, 446.02969. ESI-MS (–, MeOH): 440.02112, 442.01813, 444.01529 $[M–H]^–$, 396.03128 $[M–CO_2–H]^–$. Calcd. for $[C_{21}H_{13}Cl_2N_3O_4–H]^–$: 440.02104, 442.01809, 444.01514. HPLC: t_R = 23.58 min, 98% purity.

4-[3,5-Bis(2-hydroxy-5-methoxyphenyl)-1*H*-1,2,4-triazol-1-yl]benzoic acid (3e). In a variation of a reported procedure,[52] 300 mg (1.00 mmol, 1.0 eq) 2-(2-hydroxy-5-methoxyphenyl)-6-methoxy-4*H*-1,3-benzoxazin-4-one **6e** and 168 mg (1.10 mmol, 1.1 eq) 4-hydrazinylbenzoic acid **7a** were suspended in 3.60 mL of methanol. The mixture was brought to reflux, where it rapidly became a clear reddish-brown solution. After 3.5 hours, stirring was stopped and the mixture cooled to room temperature, when little brown solid material formed. Crystallization was completed over night in a refrigerator. The brownish crystals were collected by suction filtration, washed with methanol, dried *in vacuo*, and identified as the desired product.

Yield, 18% of pale brown crystals; M. p.: 204°C (decomp.); ^{1}H-NMR (400 MHz, DMSO-d_6, δ [ppm]): 13.07 (br s, 1H), 10.35 (s, 1H), 9.53 (s, 1H), 8.00 (d, J = 8.6 Hz, 2H), 7.58 (d, J = 8.6 Hz, 2H), 7.52 (d, J = 2.4 Hz, 1H), 7.12 (d, J = 3.1 Hz, 1H), 7.04–6.92 (m, 3H), 6.78 (d, J = 8.9 Hz, 1H), 3.77 (s, 3H), 3.72 (s, 3H). ^{13}C-NMR (101 MHz, DMSO-d_6, δ [ppm]): 166.5, 159.8, 152.3, 152.0, 152.0, 150.4, 149.0, 141.2, 130.6, 130.3, 123.5, 118.7, 118.5, 118.1, 117.1, 115.2, 114.5, 113.6, 109.8, 55.6, 55.5. ESI-MS (+, MeOH): 434.13467 $[M+H]^+$, 456.11658 $[M+Na]^+$. Calcd. for $[C_{23}H_{19}N_3O_6+H]^+$: 434.13466. ESI-MS (–, MeOH): 432.12024 $[M–H]^–$, 388.13055 $[M–CO_2–H]^–$, 373.10703 $[M–CO_2–CH_3–H]^–$). Calcd. for $[C_{23}H_{19}N_3O_6–H]^–$ 432.12011. HPLC: t_R = 21.71 min, 98% purity.

4-[3,5-Bis(5-fluoro-2-hydroxyphenyl)-1*H*-1,2,4-triazol-1-yl]benzoic acid (3f). As a variation of the reported procedure,[52] 400 mg (1.45 mmol, 1.0 eq) 5-fluoro-*N*-(5-fluoro-2-hydroxybenzoyl)-2-hydroxybenzamide **8** and 265 mg (1.74 mmol, 1.2 eq) 4-hydrazinylbenzoic acid **7a** were suspended in 5.00 mL of ethanol. The mixture was refluxed for 8 h. Upon cooling to room temperature, a light brown solid material formed. Precipitation was completed over night in a refrigerator. The solid material was collected by suction filtration, washed with cold ethanol, and dried *in vacuo*, yielding the desired product. Yield, 13% of a light brown powder; M. p.: 221°C; ^{1}H-NMR (400 MHz, DMSO-d_6, δ [ppm]): 13.23 (br s, 1H), 10.51 (s, 1H), 10.05 (s, 1H), 8.06–7.97 (m, 2H), 7.75 (dd, J = 9.2, 3.2 Hz, 1H), 7.64–7.55 (m, 2H), 7.47 (dd, J = 8.7, 3.3 Hz, 1H), 7.32-7.20 (m, 2H), 7.07 (dd, J = 9.1, 4.7 Hz, 1H), 6.85 (dd, J = 9.1, 4.6 Hz, 1H). ^{13}C-NMR (101 MHz, DMSO-d_6, δ [ppm]): 166.81, 159.47 (d, J = 2.6 Hz), 155.78 (d, J = 234.9 Hz), 155.35 (d, J = 235.5 Hz), 152.99 (d, J = 1.6 Hz), 152.05 (d, J = 1.4 Hz), 151.56 (d, J = 2.1 Hz), 141.32, 131.18, 130.76, 123.87, 119.75 (d, J = 22.7 Hz), 119.00 (d, J = 8.1 Hz), 118.78 (d, J = 23.3 Hz), 117.78, 117.61 (d, J = 17.5 Hz), 115.32 (d, J = 8.7 Hz), 114.70 (d, J =

8.3 Hz), 112.71 (d, J = 24.7 Hz). ^{19}F-NMR (376 MHz, DMSO-d_6, δ [ppm]): -124.33 – -124.41 (m, 1F), -124.86 – -124.94 (m, 1F). ESI-MS (–, MeOH): 408.0802 [M–H]$^-$, 364.0905 [M–CO_2–H]$^-$). Calcd. for [$C_{21}H_{13}F_2N_3O_4$-H]$^-$: 408.0801. HPLC: t_R = 22.51 min, 97% purity.

(E)-2-((2-Phenylhydrazineylidene)methyl)pyridine (10). To a stirred solution of picolinaldehyde **9** (444 µL, 4.62 mmol, 1.0 eq.) and phenylhydrazine hydrochloride **7b** (675 mg, 4.62 mmol, 1.0 eq.) in absolute ethanol (9 mL) was added AcOH (133 µl, 2.31 mmol, 0.5 eq.). The mixture was heated to reflux (100°C) for 4 h. After completion of the reaction according to TLC, the volatiles were removed *in vacuo* and the newly obtain hydrazone **10** was subjected to the next step without further purification.

2-(1-Phenyl-3-(pyridin-2-yl)-1*H*-1,2,4-triazol-5-yl)phenol (12a). Molecular iodine (129 mg, 0.50 mmol, 0.2 eq.) and *tert*-butyl hydroperoxide (70% aq. solution, 1.04 mL, 7.53 mmol, 3.0 eq.) were added to a solution of hydrazone **10** (500 mg, 2.51 mmol, 1.0 eq.) and 2-(aminomethyl)phenol **11a** (937 mg, 7.53 mmol, 3.0 eq.) in dry acetonitrile (8 mL). The mixture was stirred at 90°C under air for 4 hours. After completion of the reaction, the mixture was extracted three times using sat. $Na_2S_2O_3$/EtOAc and the combined organic phases were dried over anhydrous Na_2SO_4, filtered over cotton and the solvent was removed *in vacuo* to provide the crude product, which was purified by flash column chromatography on silica gel using CH_2Cl_2/EtOAc (98:2 → 80:20) as eluent. Preparative thin-layer chromatography (pTLC with 2000 µM, 40 mg in 700 µl CH_2Cl_2 for loading and CH_2Cl_2/EtOAc 95:5, double elution) was performed in order to obtain **12a** as a light orange solid of sufficient purity. Yield, 8%; 41 mg of less pure solid were also isolated. ^{1}H-NMR (400 MHz, DMSO-d_6, δ [ppm]): 10.12 (s, 1H, OH), 8.71 (ddd, J = 4.8, 1.8, 1.0 Hz, 1H), 8.16 (dt, J = 7.7 Hz, 1.0 Hz, 1H), 7.96 (td, J = 7.7, 1.8 Hz, 1H), 7.48 (ddd, J = 7.7, 4.8, 1.0 Hz, 1H), 7.43–7.46 (m, 5H), 7.40–7.42 (m, 1H, H), 7.34 (ddd,

J = 8.2, 7.6, 1.6 Hz, 1H), 6.91 (td, J = 7.6, 0.9 Hz, 1H), 6.87 (dd, J = 8.2, 0.9 Hz, 1H). ^{13}C-NMR (101 MHz, DMSO-d_6, δ [ppm]): 160.4, 155.5, 153.0, 149.8, 149.2, 138.3, 137.2, 132.0, 130.7, 129.2, 128.4, 124.3, 123.7, 121.8, 119.1, 116.1, 115.3. ESI-MS (+, MeOH): 315.1240 $[M+H]^+$, 337.1059 $[M+Na]^+$. Calcd. for $[C_{19}H_{14}N_4O+H]^+$: 315.1240. HPLC: t_R = 17.27 min, 93% purity.

2-(1,5-Diphenyl-1H-1,2,4-triazol-3-yl)pyridine (12b). Molecular iodine (129 mg, 0.50 mmol, 0.20 eq.) and *tert*-butyl hydroperoxide (70% aq. solution, 1.04 mL, 7.53 mmol, 3.0 eq.) were added to a solution of hydrazone **10** (500 mg, 2.51 mmol, 1.0 eq.) and benzylamine **11b** (831 µL, 7.53 mmol, 3.0 eq.) in dry acetonitrile (8 mL). The mixture was stirred at 90°C under air for 4 hours. After completion of the reaction, the mixture was extracted three times using sat. $Na_2S_2O_3$/EtOAc, and the combined organic phases were dried over anhydrous Na_2SO_4, filtered over cotton and the solvent was removed *in vacuo* to provide the crude product, which was purified by flash column chromatography on silica gel using CH_2Cl_2/EtOAc (98:2 → 80:20) as eluent in order to obtain the desired product as a beige crystal. Yield, 2%; 291 mg of less pure solid were also isolated. ^{1}H-NMR (400 MHz, DMSO-d_6, δ [ppm]): 8.71 (ddd, J = 4.8, 2.0, 1.1 Hz, 1H), 8.18 (dt, J = 7.9, 1.1 Hz, 1H), 7.96 (td, J = 7.9, 2.0 Hz, 1H), 7.55–7.42 (m, 11H). ^{13}C-NMR (101 MHz, DMSO-d_6, δ [ppm]): 160.7, 154.6, 149.8, 149.2, 137.9, 137.2, 130.3, 129.6, 129.4, 128.7, 128.7, 127.5, 125.8, 124.4, 121.9. ESI-MS (+, MeOH): 299.1293 $[M+H]^+$, 321.1112 $[M+H]^+$. Calcd. for $[C_{19}H_{14}N_4+H]^+$: 299.1291. HPLC: t_R = 17.75 min, 98% purity.

ASSOCIATED CONTENT

Supporting Information available: This material is available free of charge via the internet. It includes further enzyme inhibition data (MS), enzyme kinetic analyses, detailed EPR spectroscopic analyses, NMR binding experiments of control compounds, docking structures, as well as further analyses of the cellular effects of deferasirox (cell proliferation, western blots, immunostaining). Additional experimental methods are presented.

AUTHOR INFORMATION

Corresponding Author

* phone: +49 761 203-4896, fax: +49 761 203-6321, e-mail: manfred.jung@pharmazie.uni-freiburg.de

ORCID

Martin Roatsch: 0000-0002-9274-1433, Nicolas P. F. Barthes: 0000-0002-5102-3056, Manfred Jung: 0000-0002-6361-7716.

Present Address

† Martin Roatsch: University of Copenhagen, Center for Biopharmaceuticals, Universitetsparken 2, 2100 København Ø, Denmark

Author Contributions

The manuscript was written through contributions of all authors. All authors have given approval to the final version of the manuscript.

Notes

The authors declare no competing financial interest.

ACKNOWLEDGMENT

We thank K. Schmidtkunz (Albert-Ludwigs-University Freiburg) and F. Beier (Medical Center – University of Freiburg) for assistance with cell culture. Research on inhibitors of JmjC KDMs was funded by the Collaborative Research Center 992 MEDEP "Medical Epigenetics" (Projects A04 to M. Jung, B01 to R. Schüle, and C03 to S. Lassmann). R. Schüle was further supported by grants from the European Research Council (AdGrant 322844) and the Deutsche Forschungsgemeinschaft (DFG) (CRC 850, CRC 746, and SCHU688/12-1). S. Lassmann was further supported by the DFG (CRC 850, projects C5 and Z1) and the German Cancer Consortium Partner Site Freiburg (Program Molecular Diagnostics). C. J. Schofield and A. Kawamura acknowledge Cancer Research UK (C8717/A18245) and the BHF Centre of Research Excellence Oxford (RE/08/004/23915). A. Kawamura is further supported by the Royal Society Dorothy Hodgkin Fellowship. E. Schleicher thanks the DFG for financial support (project SCHL1823/3-1). M. Roatsch acknowledges a doctoral scholarship from the Studienstiftung des deutschen Volkes and a research fellowship from the DFG (RO5526/1-1). K.-F. Hsu and M. I. Abboud acknowledge support from the Ministry of National Defense, Medical Affairs Bureau, Taiwan, and the Biochemical Society Krebs Memorial Award, respectively. We thank the COST action EpiChemBio (CM1406) for support.

REFERENCES

[1] Arrowsmith, C. H., Bountra, C., Fish, P. V., Lee, K., and Schapira, M. (2012) Epigenetic protein families: a new frontier for drug discovery, *Nat. Rev. Drug Discov. 11*, 384-400.

[2] Kouzarides, T. (2007) Chromatin Modifications and Their Function, *Cell 128*, 693-705.

[3] Tsukada, Y.-i., Fang, J., Erdjument-Bromage, H., Warren, M. E., Borchers, C. H., Tempst, P., and Zhang, Y. (2006) Histone demethylation by a family of JmjC domain-containing proteins, *Nature 439*, 811-816.

[4] Whetstine, J. R., Nottke, A., Lan, F., Huarte, M., Smolikov, S., Chen, Z., Spooner, E., Li, E., Zhang, G., Colaiacovo, M., and Shi, Y. (2006) Reversal of histone lysine trimethylation by the JMJD2 family of histone demethylases, *Cell 125*, 467-481.

[5] Williams, S. T., Walport, L. J., Hopkinson, R. J., Madden, S. K., Chowdhury, R., Schofield, C. J., and Kawamura, A. (2014) Studies on the catalytic domains of multiple JmjC oxygenases using peptide substrates, *Epigenetics 9*, 1596-1603.

[6] Zheng, Y.-C., Chang, J., Wang, L.-C., Ren, H.-M., Pang, J.-R., and Liu, H.-M. (2019) Lysine demethylase 5B (KDM5B): A potential anti-cancer drug target, *Eur. J. Med. Chem. 161*, 131-140.

[7] Berry, W. L., Shin, S., Lightfoot, S. A., and Janknecht, R. (2012) Oncogenic features of the JMJD2A histone demethylase in breast cancer, *Int. J. Oncol. 41*, 1701-1706.

[8] Patani, N., Jiang, W. G., Newbold, R. F., and Mokbel, K. (2011) Histone-modifier Gene Expression Profiles Are Associated with Pathological and Clinical Outcomes in Human Breast Cancer, *Anticancer Res. 31*, 4115-4125.

[9] Shin, S., and Janknecht, R. (2007) Activation of androgen receptor by histone demethylases JMJD2A and JMJD2D, *Biochem. Biophys. Res. Commun. 359*, 742-746.

[10] Kogure, M., Takawa, M., Cho, H.-S., Toyokawa, G., Hayashi, K., Tsunoda, T., Kobayashi, T., Daigo, Y., Sugiyama, M., Atomi, Y., Nakamura, Y., and Hamamoto, R. (2013) Deregulation of the histone demethylase JMJD2A is involved in human carcinogenesis through regulation of the G_1/S transition, *Cancer Lett. 336*, 76-84.

[11] Kim, T.-D., Shin, S., Berry, W. L., Oh, S., and Janknecht, R. (2012) The JMJD2A demethylase regulates apoptosis and proliferation in colon cancer cells, *J. Cell. Biochem. 113*, 1368-1376.

[12] Mallette, F. A., and Richard, S. (2012) JMJD2A Promotes Cellular Transformation by Blocking Cellular Senescence through Transcriptional Repression of the Tumor Suppressor CHD5, *Cell Rep. 2*, 1233-1243.

[13] Kauffman, E. C., Robinson, B. D., Downes, M. J., Powell, L. G., Lee, M. M., Scherr, D. S., Gudas, L. J., and Mongan, N. P. (2011) Role of androgen receptor and associated lysine-demethylase coregulators, LSD1 and JMJD2A, in localized and advanced human bladder cancer, *Mol. Carcinog. 50*, 931-944.

[14] Guerra-Calderas, L., González-Barrios, R., Herrera, L. A., Cantú de León, D., and Soto-Reyes, E. (2015) The role of the histone demethylase KDM4A in cancer, *Cancer Genet. 208*, 215-224.

[15] Chakraborty, A. A., Laukka, T., Myllykoski, M., Ringel, A. E., Booker, M. A., Tolstorukov, M. Y., Meng, Y. J., Meier, S. R., Jennings, R. B., Creech, A. L., Herbert, Z. T.,

McBrayer, S. K., Olenchock, B. A., Jaffe, J. D., Haigis, M. C., Beroukhim, R., Signoretti, S., Koivunen, P., and Kaelin, W. G. (2019) Histone demethylase KDM6A directly senses oxygen to control chromatin and cell fate, *Science 363*, 1217-1222.

[16] Spannhoff, A., Hauser, A.-T., Heinke, R., Sippl, W., and Jung, M. (2009) The Emerging Therapeutic Potential of Histone Methyltransferase and Demethylase Inhibitors, *ChemMedChem 4*, 1568-1582.

[17] McGrath, J., and Trojer, P. (2015) Targeting histone lysine methylation in cancer, *Pharmacol. Ther. 150*, 1-22.

[18] Butler, J. S., Koutelou, E., Schibler, A. C., and Dent, S. Y. R. (2012) Histone-modifying enzymes: regulators of developmental decisions and drivers of human disease, *Epigenomics 4*, 163-177.

[19] Hoffmann, I., Roatsch, M., Schmitt, M. L., Carlino, L., Pippel, M., Sippl, W., and Jung, M. (2012) The role of histone demethylases in cancer therapy, *Mol. Oncol. 6*, 683-703.

[20] Johansson, C., Tumber, A., Che, K., Cain, P., Nowak, R., Gileadi, C., and Oppermann, U. (2014) The roles of Jumonji-type oxygenases in human disease, *Epigenomics 6*, 89-120.

[21] Rüger, N., Roatsch, M., Emmrich, T., Franz, H., Schüle, R., Jung, M., and Link, A. (2015) Tetrazolylhydrazides as Selective Fragment-Like Inhibitors of the JumonjiC-Domain-Containing Histone Demethylase KDM4A, *ChemMedChem 10*, 1875-1883.

[22] Roatsch, M., Robaa, D., Pippel, M., Nettleship, J. E., Reddivari, Y., Bird, L. E., Hoffmann, I., Franz, H., Owens, R. J., Schüle, R., Flaig, R., Sippl, W., and Jung, M. (2016)

Substituted 2-(2-aminopyrimidin-4-yl)pyridine-4-carboxylates as potent inhibitors of JumonjiC domain-containing histone demethylases, *Future Med. Chem. 8*, 1553-1571.

[23] Morera, L., Roatsch, M., Fürst, M. C. D., Hoffmann, I., Senger, J., Hau, M., Franz, H., Schüle, R., Heinrich, M. R., and Jung, M. (2016) 4-Biphenylalanine- and 3-Phenyltyrosine-Derived Hydroxamic Acids as Inhibitors of the JumonjiC-Domain-Containing Histone Demethylase KDM4A, *ChemMedChem 11*, 2063-2083.

[24] Rose, N. R., Ng, S. S., Mecinović, J., Liénard, B. M. R., Bello, S. H., Sun, Z., McDonough, M. A., Oppermann, U., and Schofield, C. J. (2008) Inhibitor Scaffolds for 2-Oxoglutarate-Dependent Histone Lysine Demethylases, *J. Med. Chem. 51*, 7053-7056.

[25] Guillade, L., Sarno, F., Tarhonskaya, H., Nebbioso, A., Alvarez, S., Kawamura, A., Schofield, C. J., Altucci, L., and de Lera, A. R. (2018) Synthesis and Biological Evaluation of Tripartin, a Putative KDM4 Natural Product Inhibitor, and 1-Dichloromethylinden-1-ol Analogues, *ChemMedChem 13*, 1949-1956.

[26] King, O. N. F., Li, X. S., Sakurai, M., Kawamura, A., Rose, N. R., Ng, S. S., Quinn, A. M., Rai, G., Mott, B. T., Beswick, P., Klose, R. J., Oppermann, U., Jadhav, A., Heightman, T. D., Maloney, D. J., Schofield, C. J., and Simeonov, A. (2010) Quantitative High-Throughput Screening Identifies 8-Hydroxyquinolines as Cell-Active Histone Demethylase Inhibitors, *PLoS One 5*, e15535.

[27] Rotili, D., Tomassi, S., Conte, M., Benedetti, R., Tortorici, M., Ciossani, G., Valente, S., Marrocco, B., Labella, D., Novellino, E., Mattevi, A., Altucci, L., Tumber, A., Yapp, C., King, O. N. F., Hopkinson, R. J., Kawamura, A., Schofield, C. J., and Mai, A. (2014) Pan-Histone

Demethylase Inhibitors Simultaneously Targeting Jumonji C and Lysine-Specific Demethylases Display High Anticancer Activities, *J. Med. Chem. 57*, 42-55.

[28] Kruidenier, L., Chung, C.-w., Cheng, Z., Liddle, J., Che, K., Joberty, G., Bantscheff, M., Bountra, C., Bridges, A., Diallo, H., Eberhard, D., Hutchinson, S., Jones, E., Katso, R., Leveridge, M., Mander, P. K., Mosley, J., Ramirez-Molina, C., Rowland, P., Schofield, C. J., Sheppard, R. J., Smith, J. E., Swales, C., Tanner, R., Thomas, P., Tumber, A., Drewes, G., Oppermann, U., Patel, D. J., Lee, K., and Wilson, D. M. (2012) A selective jumonji H3K27 demethylase inhibitor modulates the proinflammatory macrophage response, *Nature 488*, 404-408.

[29] Leurs, U., Clausen, R. P., Kristensen, J. L., and Lohse, B. (2012) Inhibitor scaffold for the histone lysine demethylase KDM4C (JMJD2C), *Bioorg. Med. Chem. Lett. 22*, 5811-5813.

[30] Luo, X., Liu, Y., Kubicek, S., Myllyharju, J., Tumber, A., Ng, S., Che, K. H., Podoll, J., Heightman, T. D., Oppermann, U., Schreiber, S. L., and Wang, X. (2011) A Selective Inhibitor and Probe of the Cellular Functions of Jumonji C Domain-Containing Histone Demethylases, *J. Am. Chem. Soc. 133*, 9451-9456.

[31] Hamada, S., Suzuki, T., Mino, K., Koseki, K., Oehme, F., Flamme, I., Ozasa, H., Itoh, Y., Ogasawara, D., Komaarashi, H., Kato, A., Tsumoto, H., Nakagawa, H., Hasegawa, M., Sasaki, R., Mizukami, T., and Miyata, N. (2010) Design, Synthesis, Enzyme-Inhibitory Activity, and Effect on Human Cancer Cells of a Novel Series of Jumonji Domain-Containing Protein 2 Histone Demethylase Inhibitors, *J. Med. Chem. 53*, 5629-5638.

[32] Franci, G., Sarno, F., Nebbioso, A., and Altucci, L. (2017) Identification and characterization of PKF118-310 as a KDM4A inhibitor, *Epigenetics 12*, 198-205.

[33] Wang, L., Chang, J., Varghese, D., Dellinger, M., Kumar, S., Best, A. M., Ruiz, J., Bruick, R., Peña-Llopis, S., Xu, J., Babinski, D. J., Frantz, D. E., Brekken, R. A., Quinn, A. M., Simeonov, A., Easmon, J., and Martinez, E. D. (2013) A small molecule modulates Jumonji histone demethylase activity and selectively inhibits cancer growth, *Nat. Commun. 4*, 2035.

[34] Esposito, C., Wiedmer, L., and Caflish, A. (2018) In Silico Identification of JMJD3 Demethylase Inhibitors, *J. Chem. Inf. Model. 58*, 2151-2163.

[35] Jaikhan, P., Buranrat, B., Itoh, Y., Chotitumnavee, J., Kurohara, T., and Suzuki, T. (2019) Identification of ortho-hydroxy anilide as a novel scaffold for lysine demethylase 5 inhibitors, *Bioorg. Med. Chem. Lett. 29*, 1173-1176.

[36] McAllister, T. E., England, K. S., Hopkinson, R. J., Brennan, P. E., Kawamura, A., and Schofield, C. J. (2016) Recent Progress in Histone Demethylase Inhibitors, *J. Med. Chem. 59*, 1308-1329.

[37] Lohse, B., Kristensen, J. L., Kristensen, L. H., Agger, K., Helin, K., Gajhede, M., and Clausen, R. P. (2011) Inhibitors of histone demethylases, *Bioorg. Med. Chem. 19*, 3625-3636.

[38] Jambhekar, A., Anastas, J. N., and Shi, Y. (2017) Histone Lysine Demethylase Inhibitors, *Cold Spring Harbor Perspect. Med. 7*, a026484.

[39] Hauser, A.-T., Roatsch, M., Schulz-Fincke, J., Robaa, D., Sippl, W., and Jung, M. (2015) Discovery of Histone Demethylase Inhibitors, in *Epigenetic Technological Applications* (Zheng, Y. G., Ed.), pp 397-424, Academic Press, Amsterdam.

[40] Højrup, C., Coleman, O. D., Bukowski, J.-P., Clausen, R. P., and Kawamura, A. (2019) JmjC-domain-Containing Histone Demethylases, in *Epigenetic Drug Discovery* (Sippl, W., and Jung, M., Eds.), pp 265-298, Wiley-VCH, Weinheim.

[41] Horton, J. R., Woodcock, C. B., Chen, Q., Liu, X., Zhang, X., Shanks, J., Rai, G., Mott, B. T., Jansen, D. J., Kales, S. C., Henderson, M. J., Cyr, M., Pohida, K., Hu, X., Shah, P., Xu, X., Jadhav, A., Maloney, D. J., Hall, M. D., Simeonov, A., Fu, H., Vertino, P. M., and Cheng, X. (2018) Structure-Based Engineering of Irreversible Inhibitors against Histone Lysine Demethylase KDM5A, *J. Med. Chem. 61*, 10588-10601.

[42] Vazquez-Rodriguez, S., Wright, M., Rogers, C. M., Cribbs, A. P., Velupillai, S., Philpott, M., Lee, H., Dunford, J. E., Huber, K. V. M., Robers, M. B., Vasta, J. D., Thezenas, M.-L., Bonham, S., Kessler, B., Bennett, J., Fedorov, O., Raynaud, F., Donovan, A., Blagg, J., Bavetsias, V., Oppermann, U., Bountra, C., Kawamura, A., and Brennan, P. (2019) Design, Synthesis and Characterization of Covalent KDM5 Inhibitors, *Angew. Chem. Int. Ed. Engl. 58*, 515-519.

[43] Bonnici, J., Tumber, A., Kawamura, A., and Schofield, C. J. (2018) Inhibitors of both the N-methyl lysyl- and arginyl-demethylase activities of the JmjC oxygenases, *Philos. Trans. R. Soc. B 373*, 20170071.

[44] Rombout-Sestrienkova, E., van Kraaij, M. G. J., and Koek, G. H. (2016) How we manage patients with hereditary haemochromatosis, *Br. J. Haematol. 175*, 759-770.

[45] Moukalled, N. M., Bou-Fakhredin, R., and Taher, A. T. (2018) Deferasirox: Over a Decade of Experience in Thalassemia, *Mediterr. J. Hematol. Infect. Dis. 10*, e2018066.

[46] Cascella, B., Lee, S. G., Singh, S., Jez, J. M., and Mirica, L. M. (2017) The small molecule JIB-04 disrupts O2 binding in the Fe-dependent histone demethylase KDM4A/JMJD2A, *Chem. Commun. 53*, 2174-2177.

[47] Khodaverdian, V., Tapadar, S., MacDonald, I. A., Xu, Y., Ho, P.-Y., Bridges, A., Rajpurohit, P., Sanghani, B. A., Fan, Y., Thangarayu, M., Hathaway, N. A., and Oyelere, A. K. (2019) Deferiprone: Pan-selective Histone Lysine Demethylase Inhibition Activity and Structure Activity Relationship Study, *Sci. Rep. 9*, 4802.

[48] Sekirnik, R., Rose, N. R., Thalhammer, A., Seden, P. T., Mecinović, J., and Schofield, C. J. (2009) Inhibition of the histone lysine demethylase JMJD2A by ejection of structural Zn(II), *Chem. Commun.*, 6376-6378.

[49] Hagedoorn, P.-L., Schmidt, P. P., Andersson, K. K., Hagen, W. R., Flatmark, T., and Martinez, A. (2001) The Effect of Substrate, Dihydrobiopterin, and Dopamine on the EPR Spectroscopic Properties and the Midpoint Potential of the Catalytic Iron in Recombinant Human Phenylalanine Hydroxylase, *J. Biol. Chem. 276*, 22850-22856.

[50] Solomon, E. I., Brunold, T. C., Davis, M. I., Kemsley, J. N., Lee, S.-K., Lehnert, N., Neese, F., Skulan, A. J., Yang, Y.-S., and Zhou, J. (2000) Geometric and Electronic Structure/Function Correlations in Non-Heme Iron Enzymes, *Chem. Rev. 100*, 235-349.

[51] Krzyaniak, M. D., Eser, B. E., Ellis, H. R., Fitzpatrick, P. F., and McCracken, J. (2013) Pulsed EPR Study of Amino Acid and Tetrahydropterin Binding in a Tyrosine Hydroxylase Nitric Oxide Complex: Evidence for Substrate Rearrangements in the Formation of the Oxygen-Reactive Complex, *Biochemistry 52*, 8430-8441.

[52] Patil, R. S., Charugundla, K., Neela, P. K., Pradhan, N. S., and Valgeirsson, J. (2009) Substantially pure Deferasirox and process for the preparation thereof, p 16, Patent WO 2009/147529.

[53] Steinhauser, S., Heinz, U., Bartholomä, M., Weyhermüller, T., Nick, H., and Hegetschweiler, K. (2004) Complex Formation of ICL670 and Related Ligands with Fe^{III} and Fe^{II}, *Eur J Inorg Chem*, 4177-4192.

[54] Kielar, F., Wang, Q., Boyle, P. D., and Franz, K. J. (2012) A boronate prochelator built on a triazole framework for peroxide-triggered tridentate metal binding, *Inorg Chim Acta 393*, 294-303.

[55] Stieber, F., Grether, U., and Waldmann, H. (2003) Development of the Traceless Phenylhydrazide Linker for Solid-Phase Synthesis, *Chem-Eur J 9*, 3270-3281.

[56] Salehi, S., Saljooghi, A. S., and Shiri, A. (2016) Synthesis, characterization and *in vitro* anticancer evaluations of two novel derivatives of deferasirox iron chelator, *Eur. J. Pharmacol. 781*, 209-217.

[57] Chen, Z., Li, H., Dong, W., Miao, M., and Ren, H. (2016) I_2-Catalyzed Oxidative Coupling Reactions of Hydrazones and Amines and the Application in the Synthesis of 1,3,5-Trisubstituted 1,2,4-Triazoles, *Org. Lett. 18*, 1334-1337.

[58] Abboud, M. I., McAllister, T. E., Leung, I. K. H., Chowdhury, R., Jorgensen, C., Domene, C., Mecinovic, J., Lippl, K., Hancock, R. L., Hopkinson, R. J., Kawamura, A., Claridge, T. D. W., and Schofield, C. J. (2018) 2-Oxoglutarate regulates binding of hydroxylated hypoxia-inducible factor to prolyl hydroxylase domain 2, *Chem. Commun. 54*, 3130-3133.

[59] Abboud, M. I., Hinchliffe, P., Brem, J., Macsics, R., Pfeffer, I., Makena, A., Umland, K. D., Rydzik, A. M., Li, G. B., Spencer, J., Claridge, T. D., and Schofield, C. J. (2017) 19F-NMR Reveals the Role of Mobile Loops in Product and Inhibitor Binding by the Sao Paulo Metallo-beta-Lactamase, *Angew. Chem. Int. Ed. Engl. 56*, 3862-3866.

[60] Cho, E. A., Song, H. K., Lee, S. H., Chung, B. H., Lim, H. M., and Lee, M. K. (2013) Differential in vitro and cellular effects of iron chelators for hypoxia inducible factor hydroxylases, *J. Cell. Biochem. 114*, 864-873.

[61] Ford, S. J., Obeidy, P., Lovejoy, D. B., Bedford, M., Nichols, L., Chadwick, C., Tucker, O., Lui, G. Y. L., Kalinowski, D. S., Jansson, P. J., Iqbal, T. H., Alderson, D., Richardson, D. R., and Tselepis, C. (2013) Deferasirox (ICL670A) effectively inhibits oesophageal cancer growth *in vitro* and *in vivo*, *Br. J. Pharmacol. 168*, 1316-1328.

[62] Pogribny, I. P., Tryndyak, V. P., Pogribna, M., Shpyleva, S., Surratt, G., Gamboa da Costa, G., and Beland, F. A. (2013) Modulation of intracellular iron metabolism by iron chelation affects chromatin remodeling proteins and corresponding epigenetic modifications in breast cancer cells and increases their sensitivity to chemotherapeutic agents, *Int. J. Oncol. 42*, 1822-1832.

[63] Lee, D.-H., Jang, P. S., Chung, N. G., Cho, B., Jeong, D. C., and Kim, H. K. (2013) Deferasirox shows in vitro and in vivo antileukemic effects on murine leukemic cell lines regardless of iron status, *Exp. Hematol. 41*, 539-546.

[64] Choi, J. H., Kim, J. S., Won, Y. W., Uhm, J., Park, B. B., and Lee, Y. Y. (2016) The potential of deferasirox as a novel therapeutic modality in gastric cancer, *World J. Surg. Oncol. 14*, 77.

[65] Zeidan, A. M., Hendrick, F., Friedmann, E., Baer, M. R., Gore, S. D., Sasane, M., Paley, C., and Davidoff, A. J. (2015) Deferasirox therapy is associated with reduced mortality risk in a medicare population with myelodysplastic syndromes, *J. Comp. Eff. Res. 4*, 327-340.

[66] Zeidan, A. M., and Griffiths, E. A. (2018) To chelate or not to chelate in MDS: That is the question!, *Blood Rev. 32*, 368-377.

[67] Keeler, B. D., and Brookes, M. J. (2013) Iron chelation: a potential therapeutic strategy in oesophageal cancer, *Br. J. Pharmacol. 168*, 1313-1315.

[68] Bedford, M. R., Ford, S. J., Horniblow, R. D., Iqbal, T. H., and Tselepis, C. (2013) Iron Chelation in the Treatment of Cancer: A New Role for Deferasirox?, *J. Clin. Pharmacol. 53*, 885-891.

[69] Lui, G. Y. L., Obeidy, P., Ford, S. J., Tselepis, C., Sharp, D. M., Jansson, P. J., Kalinowski, D. S., Kovacevic, Z., Lovejoy, D. B., and Richardson, D. R. (2013) The Iron Chelator, Deferasirox, as a Novel Strategy for Cancer Treatment: Oral Activity Against Human Lung Tumor Xenografts and Molecular Mechanism of Action, *Mol. Pharmacol. 83*, 179-190.

[70] Dalvit, C., Fogliatto, G., Stewart, A., Veronesi, M., and Stockman, B. (2001) WaterLOGSY as a method for primary NMR screening: Practical aspects and range of applicability, *J. Biomol. NMR 21*, 349-359.

[71] Klose, R. J., Yamane, K., Bae, Y., Zhang, D., Erdjument-Bromage, H., Tempst, P., Wong, J., and Zhang, Y. (2006) The transcriptional repressor JHDM3A demethylates trimethyl histone H3 lysine 9 and lysine 36, *Nature 442*, 312-316.